The role of the intraspecific variability of hydraulic traits for modelling the plant water use in different European forest ecosystems

C.D. Jiménez-Rodríguez[1], M. Sulis[1], and S. Schymanski[1]

[1]Environmental Research and Innovation (ERIN) Department, Luxembourg Institute of Science and Technology (LIST), Belvaux, 4422, Luxembourg.

Corresponding author: César Jiménez-Rodríguez (cesar.jimenez@list.lu, cdjimenezcr@gmail.com)

Key Points:

- We explore the impact of the intraspecific variability of plant hydraulic traits on the simulated transpiration by CLM5.
- We find that a choice of plant hydraulic traits that reproduces observed plant transpiration also reduces simulated water stress.
- We demonstrate the critical role of the maximum xylem conductance in the model and its dependency on factors other than vegetation type.

Abstract

The drought resilience of forest ecosystems is generally believed to depend on the dominant tree species' hydraulic traits. These traits define the maximum water transport capacity and the degree of vulnerability to hydraulic failure of a tree species. This work evaluates the effect of the intraspecific variability of hydraulic traits on the simulated tree water use in the Community Land Model (CLM, version 5.0). We selected two contrasting broadleaved tree species and performed a series of numerical experiments by modifying the parameters of the plant vulnerability curve and the maximum xylem hydraulic conductance accounting for the variability within each species. Our prescribed parameter sets represent vulnerable and resistant tree responses to the water deficit. At sites with an ample water supply, the resistant configuration simulates reduced water stress and increased transpiration compared to the vulnerable configuration. Meanwhile, the model results are counter-intuitive at temporarily dry sites when water availability is the limiting factor. The numerical experiments demonstrate the emergent role of the maximum xylem conductance as a modulator of the plant water use strategy and the simulated transpiration within the model. Using the default value for maximum xylem conductance, the model tends to overestimate the early summer transpiration at drier sites, forcing the vegetation to experience unrealistic water stress later in the year. Our findings suggest that the parameterization of maximum xylem conductance is an important yet unresolved problem in the CLM and similar land surface models.

Plain Language Summary

The survival of trees in drought conditions depends on their ability to adapt to water scarcity. Part of this adaptation is characterized by specific plant traits, which are an important component of Land Surface Models and largely determine the relationship between soil moisture and canopy gas exchange. Our study explores how the variability of specific plant traits of individual tree species may affect the selected model's ability to reproduce the water use observed in forest stands in Europe. For climates with a pronounced summer dry period, we found that the default model settings overestimated the vegetation water use in the early growing season, when water is abundant, resulting in severe water stress and underestimated transpiration as the dry season progressed. We specifically demonstrate that a rarely considered plant trait, representing the maximum water transport capacity, plays an essential role in controlling the magnitude of simulated water use and that adjustments to this parameter greatly help to reproduce the vegetation water use observed in seasonally dry climates.

1 Introduction

The recent worldwide increase in drought incidence and severity (He et al., 2020) has been associated with alterations in the soil carbon and nitrogen dynamics (Deng et al., 2021), high rates of tree mortality (Powers et al., 2020; Senf et al., 2020) as a consequence of the high atmospheric water demand (Hammond et al., 2022; McDowell et al., 2022), and a diminution in forest evaporation (Lansu et al., 2020; Lindroth et al., 2020). The severity of drought impacts on forest ecosystems and the spatial extent of them depends on the vegetation resistance and resilience to water scarcity. The latter reflects the admixed vulnerability of individual trees (Haberstroh & Werner, 2022) and is partly driven by the safety mechanisms used to overcome disturbances in the whole tree hydraulic system (Arend et al., 2022).

The resistance of a species to water stress is commonly expressed in the plant vulnerability curve and the recovery patterns shown by the tree species (Klein et al., 2018). This curve postulates a continuous decline of plant organ conductance (e.g., roots, branches, leaves) with declining water pressure in the plant organ (Sperry & Love, 2015; Venturas et al., 2017). The parameters of the curve differ among and within tree species (Rosner et al., 2019), and are influenced by the provenance of the species (Hajek et al., 2016; Lobo et al., 2018) and xylem features (Pereira et al., 2018). The plant vulnerability curve has been analyzed across species and biomes (Choat et al., 2012), allowing the degree of vulnerability to hydraulic failure to be quantified (Venturas et al., 2017). Vulnerable trees commonly have a low wood density, an early loss of conductance, and a small threshold between unstressed conditions and the occurrence of hydraulic damage. Resistant trees have vulnerability curves ranging from gradual to steep responses at lower water potentials. These trees commonly have large safety margins and high wood density (Johnson et al., 2012; Meinzer & McCulloh, 2013; Mrad et al., 2019). The degree of vulnerability to hydraulic failure has been related to the trade-off between xylem safety and efficiency for many tree species (U. G. Hacke et al., 2006; Venturas et al., 2017). This trade-off requires the coordination of the plant hydraulic traits and water use strategy (WUS), which ranges from aggressive to conservative (Flo et al., 2021; Mrad et al., 2019). Also, the WUS is influenced by the stomatal regulation capacity of the tree species (Konings & Gentine, 2017), modulated by the vapor pressure deficit (Novick et al., 2019), and driven partially by the soil water content (Fu et al., 2022). However, the current evidence does not allow the generalization of this trade-off for all plant species (Gleason et al., 2016).

The plant hydraulic theory is numerically implemented in models using either a plant pipe model, a porous media model, an electrical analogy model (Li et al., 2021), or optimality-based models (Sabot et al., 2020; H. Xu et al., 2021). Plant pipe models follow the Hagen-Poiseulle law and require the use of allometric scaling laws (Li et al., 2021; Mrad et al., 2018), whereas porous media models are based on Richards equation assuming that water movement through the xylem mimics an unsaturated porous media flow (Christoffersen et al., 2016; Li et al., 2021). The electrical analogy models resemble an electrical circuit with resistance and capacitance parameters that control the water flow following Darcy's law (Bonan et al., 2014; Li et al., 2021). Finally, optimality-based models do not prescribe hydraulic traits based on observations, but assume that vegetation finds its “optimum” by maximizing a carbon-related goal function for given environmental conditions (Joshi et al., 2022; Sabot et al., 2020). An electrical analogy model has low to moderate computational requirements making it a suitable model for implementation in large scale Land Surface Models (LSMs). For example, the Community Land Model 5.0 (CLM5, Lawrence et al., 2019) implements an electrical analogy model using the plant vulnerability curve to downscale the segment conductance according to the percent loss of conductance (PLC) (Kennedy et al., 2019). Given its recent implementation, the simulated plant hydraulic response (e.g., vulnerability to hydraulic failure) of CLM5 during drought conditions and across different forested ecosystems has not yet been evaluated in detail. Specifically, it has never been examined in detail to what extent the current (and default) plant hydraulic formulation and parameterization of the model reproduces realistic transpiration rates and plant water status under varying soil moisture availability and atmospheric water demand.

The implementation of plant hydraulic formulations for LSMs from a species-specific perspective is rare (e.g., De Kauwe et al., 2022; Sabot et al., 2020), and most of the current LSMs rely on the definition of plant hydraulic traits within the Plant Functional Type (PFT) classification framework (e.g., D. M. Lawrence et al., 2019; Zhang et al., 2022) . This

classification assumes that hydraulic traits are spatially homogeneous and temporally fixed within predefined vegetation categories, which is equivalent to assuming the same drought sensitivity within the same PFT class. Several studies have addressed the implications associated with the loss of diversity in the PFT classification in terms of water and carbon dynamics by using deterministic or stochastic coordinated plant attributes (Christoffersen et al., 2016; Pappas et al., 2016; Y. P. Wang et al., 2012; X. Xu et al., 2016) or by exploiting plant trait-climate relationships (Verheijen et al., 2013). A recent study by Butler et al. (2022) showed that the aggregation of allocation and hydraulic traits into PFTs reduces the productivity of the modelled ecosystem with respect to the flux data of sites with a strong dependency on vegetation phenology. Liu et al. (2021) argues the negative impacts of generalizing the plant hydraulic traits at PFT level and proposed a set of hydraulic functional types as an alternative to current PFTs. Overall, representing the plant trait inter- and intraspecific diversity within the PFT broad classification scheme remains a challenging task requiring the characterization of the emergent plant response by coordinating water use strategies with the xylem vulnerability (Skelton et al., 2015). While the trade-off between plant hydraulic traits has been addressed in previous studies using detailed plant hydrodynamic models (e.g., Mirfenderesgi et al. (2019)), the coordination between hydraulic traits and water use strategies remains largely unexplored, with some attempts carried out aiming to improve the plant hydraulic framework implemented in LSMs (e.g., Eller et al., 2020; Sabot et al., 2020). Addressing this issue may provide an opportunity to define optimal strategies for large-scale parameterizations of key plant hydraulic traits (e.g., maximum xylem conductance), which are rarely documented in existing hydraulic trait databases (Liu et al., 2021).

This manuscript aims to evaluate the effect of the intraspecific variability of plant hydraulic traits on the simulated transpiration response of two contrasting tree species in CLM5. The intraspecific variability of plant hydraulic traits defines the spectrum of vulnerability responses to hydraulic failure and the water use strategies of each species. This spectrum considers that individual tree species have different boundaries determining their degree of vulnerability to hydraulic failure. Our hypothesis is that vulnerable trees transpire more than resistant trees under unstressed water conditions and strongly reduce transpiration during dry periods. On the other hand, resistant trees maintain low transpiration rates but experience less stress on the plant hydraulic system. This hypothesis is evaluated for two broadleaved tree species, *Quercus ilex* L. and *Fagus sylvatic*a L., with contrasting phenologies and provenances. For each species, we distinguish between a resistant and vulnerable hydraulic trait configuration by extracting from the reported parameter sets for that species the plant vulnerability curves with the minimum and maximum xylem pressure inducing 50% loss of hydraulic conductance (Ψ_{p50}) value, respectively. The results of point-scale numerical experiments with CLM5 based on each parameterization are compared to the sap flux observed at four experimental sites across Europe. The representation of the simulated vulnerability to hydraulic failure and the water use strategy of each species are interpreted using the simulated leaf water stress factor (β) and percent loss of conductance (PLC) in different plant organs.

2 Materials and Methods

2.1 Tree Species and Experimental Sites

The tree species selected for this study, *Fagus sylvatica* L. and *Quercus ilex* L., belong to the same botanical family (Fagaceae) but differ in their phenology and spatial distribution in

Europe (Figure 1). *Fagus sylvatica* is a deciduous broadleaved tree distributed in Central and Western Europe, from Southern Italy to Southern Norway. This tree species grows from sea level to 1000 m a.s.l., with a higher upper elevation limit in dryer regions. It does not survive in locations with poor drainage or stagnant water, and its relatively shallow root system makes it susceptible to emerging hot droughts and high temperatures (Houston Durrant et al., 2016; von Wuehlisch, 2008). *Quercus ilex* is a broadleaved evergreen species that grows as a tree or shrub. It inhabits the Mediterranean basin from the coast up to 1800 m a.s.l. This species can survive low temperatures and its sclerophyllous character increases its resistance to drought by reducing water loss during dry periods (de Rigo & Caudullo, 2016; Schirone et al., 2019).

Two experimental sites for each species were selected from the SAPFLUXNET database (Poyatos et al., 2020). *Fagus sylvatica* is the dominant tree species in Hesse (France, FR-Hes) and Hinnensee (Germany, DE-Hin), over the sampling periods of 2001-2005 and 2012-2014, respectively (Table 1). Both sites have a temperate oceanic climate (Cfb) according to Köppen-Geiger's climate classification (Beck et al., 2018), with no significant intraseasonal precipitation variability. The stand age marks the main difference between these two sites; trees in FR-Hes were 34 years old during the selected measurement period while those in DE-Hin were more than 200 years old. The mean tree diameter reflects this age difference, with 12.9 cm at FR-Hes and 43.6 cm at DE-Hin. *Quercus ilex* is the dominant tree species in Puechabon (France, FR-Pue) and Alto Tajo (Spain, ES-Alt). These sites cover the monitoring periods 2001-2005 and 2012-2014, respectively. The climate differs slightly between these two sites; FR-Pue has a hot-summer Mediterranean climate (Csa) while ES-Alt has a warm-summer Mediterranean climate (Csb). The different elevations of the sites explain the differences in climate classification (Table 1). Despite a lack of differences in the stand age between these two sites, the diameter recorded for the trees in FR-Pue (9.1 cm) is much smaller than the diameter in ES-Alt (24.4 cm).

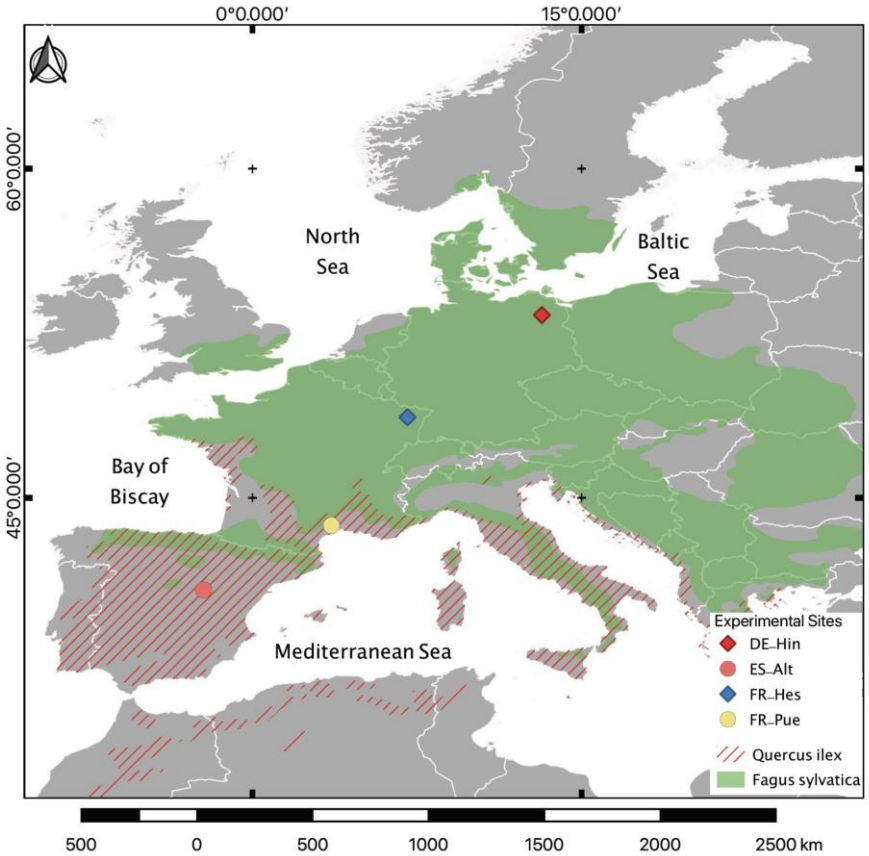

Figure 1. Geographical location of the selected experimental sites and the spatial distribution of *Fagus sylvatica* L. (diamonds) and *Quercus ilex* L. (circles) and their spatial distribution across Europe. The spatial distribution of the tree species is based on Mauri et al. (2022).

2.2 Model Setup

The Community Land Model version 5.0 (CLM5, Lawrence et al. (2019)) was applied at each experimental site using point-scale setups. Hourly atmospheric forcing was retrieved from the SAPFLUXNET dataset. This dataset includes precipitation, wind speed, air temperature, relative humidity, and incoming shortwave radiation. The incoming longwave radiation was calculated according to An et al. (2017) using the vapor pressure deficit and temperature. The COSMO-REA6 reanalysis product (Bollmeyer et al., 2015) with a temporal and spatial resolution of one hour and 0.05°, respectively, was used to fill in the missing variables (i.e., atmospheric pressure) and temporal data gaps for each site. The monthly leaf area index (LAI) in m^2 m^{-2} is based on the 8-days' time-series of the Global Land Surface Satellite (GLASS) product (Liang et al., 2013, 2014) that has a spatial resolution of 0.05° for the different periods under analysis. The monthly stem area index (SAI) in m^2 m^{-2} was retrieved from the global surface dataset of the model as described in Lawrence & Chase (2010). The LAI of the sites covered with *Fagus sylvatica* trees was forced to 0.0 m^2m^{-2} from October to April. This decision was based on the observed phenology at FR-Hes (Q. Wang et al., 2005) and DE-Hin (Blume et al., 2022). The root area index (RAI) in m^2m^{-2} is calculated in the model (see Equation 2.11.15 of the technical documentation (UCAR, 2020)) based on plant functional type-specific parameters such as the LAI, SAI, root fraction in each soil layer, and the root-to-shoot ratio. The main soil

characteristics (e.g., soil texture, organic matter content) were taken from Bonan et al. (2002), while the depth to bedrock was taken from Pelletier et al. (2016). Multi-year spin-up runs were performed for each experimental site by reinitializing soil moisture and soil temperature until a dynamic equilibrium condition was reached. The tree species at the selected sites pertain to two distinctive plant functional types (PFTs), with *Fagus sylvatica* representing the Temperate Broadleaf Deciduous Tree (BDT) in FR-Hes and DE-Hin and *Quercus ilex* representing the Temperate Broadleaf Evergreen Tree (BET) in FR-Pue and ES-Alt; see Table 2 for the default plant hydraulic configuration (DC) of these two PFTs.

2.3 Plant Vulnerability Curve

The plant vulnerability curve (PVC) implemented in CLM5 (Equation 1) determines the plant segment specific hydraulic conductance k ($mm_{H2O}\ mm_{H2O}^{-1}s^{-1}$) based on three parameters: the xylem pressure inducing 50% loss of hydraulic conductance (Ψ_{p50}, MPa), the non-dimensional sigmoidal shape parameter of the curve (c_k), and the maximum plant hydraulic conductance (k_{max}, $mm_{H2O}\ mm_{H2O}^{-1}s^{-1}$). The CLM5 plant hydraulic routine uses a plant segmentation that differentiates between roots, stems, shaded and sunlit leaves. Each plant segment uses k_{max}, Ψ_{p50} and c_k as static parameters that can be adjusted and may differ between plant segments (i.e., root, xylem, and sunlit and shaded leaf) and PFTs. The plant hydraulic system of CLM5 uses k to determine the flux per plant segment by applying a Darcy's law equation, where the reference area varies between plant segments: the leaf area index (LAI, m^2m^{-2}) for the stem-to-leaf, the stem area index (SAI, m^2m^{-2}) for the root-to-stem, and the root area index (RAI, m^2m^{-2}) for the soil-to-root segment. A detailed description of the equations used by the plant hydraulic system of CLM5 is provided in Kennedy et al. (2019) and Lawrence et al. (2019).

$$k = k_{max} 2^{-\left(\frac{\Psi}{\Psi_{p50}}\right)^{c_k}}$$	Equation 1

2.4. Intraspecific Variability of Plant Hydraulic Traits

The intraspecific variability of both tree species was determined based on the loss of hydraulic conductance by 12%, 50%, 88%, and in some cases at 10% (Ψ_{p12}, Ψ_{p50}, Ψ_{p88}, and Ψ_{p10}, respectively), as reported in the Xylem Functional Traits (XFT) database (Choat et al., 2012). The limited data for *Fagus sylvatica* in the XFT database led to the selection of additional experimental data to improve the representation of the species. Meanwhile, the data set of *Quercus ilex* was subject to an additional screening of the individual records due to concerns about the measurement of the PVC in different species of Oaks (Cochard et al., 2013) and in particular to the open-vessels artefact issue affecting the measurements in *Quercus ilex* (Martin-StPaul et al., 2014). Therefore, we conducted a literature review and selected those experiments that implemented procedures to prevent such artefacts (e.g., excised under water). The complete list of references used to retrieve the additional data for *Fagus sylvatica* and *Quercus ilex* is available in Table S1. The c_k parameter of each dataset was determined by converting the reported slope of the vulnerability curve at Ψ_{p50} to c_k or by solving the CLM vulnerability curve for c_k and inserting any provided combination of PLC and Ψ_{p10}, or Ψ_{p12}, or Ψ_{p88} values reported in the XFT database, with a preference for Ψ_{p10} or Ψ_{p12} if available. The procedure to determine the c_k parameter assumes that Equation 1 follows the Weibull distribution, allowing the

vulnerability curve formulation from Domec and Gartner (2001) to be used. From this formulation, we derived Equation 2 to calculate the c_k parameter based on the Ψ_{p50}, the slope of the curve (s) at Ψ_{p50} (Pa^{-1}), and V as a constant dimensionless value of 34.66. To determine V, we deduced Equation 3 from Domec and Gartner (2001) and inserted the percent loss of conductivity (τ_{50}) of 50%. Equation 4 is used to calculate s (Pa^{-1}) using the slope at any specific loss of conductivity (τ). This indicator is calculated with Equation 4 using τ in %, Ψ_{p50}, and Ψ_x that represents the matric potential at the selected τ. Finally, the two curves with the highest and lowest Ψ_{p50} values were selected for each species to represent the vulnerable (VC) and resistant (RC) configuration, respectively (Figure 2); see Table 2 for more details on the obtained values.

$$c_k = \frac{\Psi_{p50} \cdot s}{V}$$	Equation 2

$$V = (\tau_{50} - 100) \cdot \ln\left(1 - \frac{\tau_{50}}{100}\right)$$	Equation 3

$$s = -25 \frac{\log\left(\frac{100 - \tau}{\tau}\right)}{\Psi_x - \Psi_{p50}}$$	Equation 4

The xylem water potentials of *Fagus sylvatica* have a narrow distribution, with the Ψ_{p12}, Ψ_{p50}, and Ψ_{p88} values ranging from -2.0 MPa to -5.0 MPa (Figure 2). The two extreme curves obtained from this dataset have a steep decline of hydraulic conductance with the diminution of water potentials, with a small range in c_k (1.73 to 3.33) and Ψ_{p50} (-1.9 MPa to -4.7 MPa) values (Table 2). *Quercus ilex* has a more negative range of xylem water potentials than *Fagus sylvatica*, ranging from -4.97 MPa to -7.66 MPa. Therefore, the VC of *Quercus ilex* is described by a Ψ_{p50} of -4.97 MPa and a c_k value of 1.06; meanwhile, its RC has a Ψ_{p50} of -7.66 MPa and a c_k of 2.27.

The k_{max} values used by default in CLM5 are assumed constant for the different PFTs and homogeneous across the different plant organs (i.e., root, xylem, and leaves). k_{max} values for each plant segment can be determined based on the experimental specific hydraulic conductance (k_s, kg $m^{-2}MPa^{-1}s^{-1}$), which is defined as the flow rate per cross sectional area per unit of pressure difference along a plant segment (kg $m^{-2}MPa^{-1}s^{-1}$) (Eamus et al., 2016). However, a standard procedure for determining k_{max} for its use in CLM5 (i.e., at PFT level and for each plant segment) from tree- and plant organ-specific information existing in literature has not been specified yet. Therefore, considering the large uncertainty in estimating this parameter and the unknown effect of its variability, we arbitrarily choose a range of values between one order of magnitude above (2.0×10^{-7} mm_{H2O} $mm_{H2O}^{-1}s^{-1}$) and below (2.0×10^{-9} mm_{H2O} $mm_{H2O}^{-1}s^{-1}$) the default value (2.0×10^{-8} mm_{H2O} $mm_{H2O}^{-1}s^{-1}$) of the model. The upper and lower values of this variability range are referred to from now as high (Hk_{max}) and low (Lk_{max}) xylem conductance, respectively.

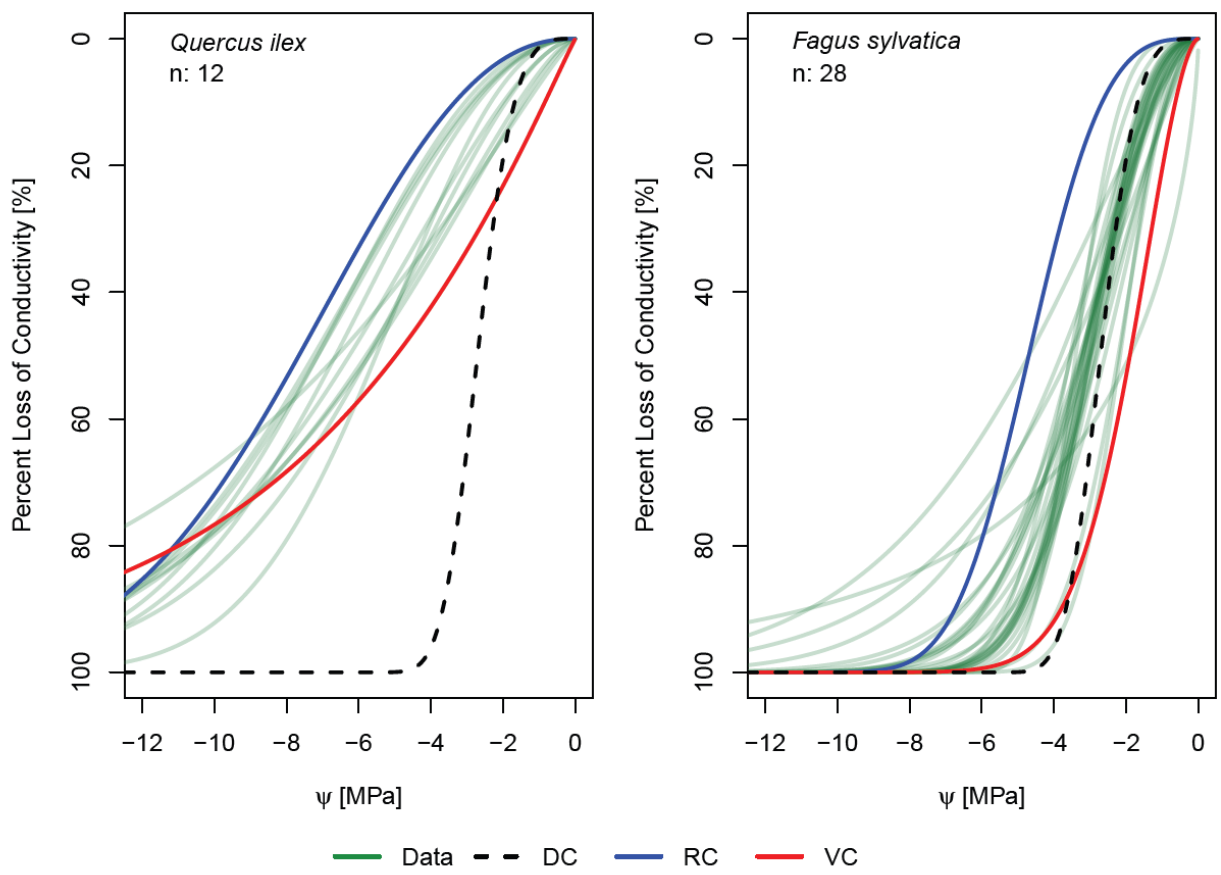

Figure 2. Spectrum of the vulnerability curves of *Quercus ilex* L. and *Fagus sylvatica* L. The solid blue, red, and dashed black lines represent the resistant (RC), vulnerable (VC), and default (DC) vulnerability curves used in the numerical experiments, respectively. The vulnerability curves were not differentiated between plant organs within the same tree species. The solid green lines show the full data set of vulnerability curves used for each species.

2.5. Numerical Experiments

The role of the intraspecific variability of plant hydraulic traits in contrasting tree species was examined based on a series of numerical experiments. These experiments aimed to assess to what extent the plant hydraulics representation of CLM5 reproduces the measured transpiration of each experimental site based on the spectrum of vulnerability to the hydraulic failure of each tree species (Table 2). All the experiments considered that the plant segments (i.e., roots, stems, leaves) of a given plant functional type (PFT) have the same plant hydraulic parameterization (i.e., k_{max}, Ψ_{p50}, and c_k); allowing the same degree of vulnerability to hydraulic failure between the distal portions of the modeled vegetation.

The first set of experiments compared the effect of the PVC shape on the distribution of PLC values, leaf water stress (β), and the transpiration simulated by the model. In this experiment we only changed the shape of the PVC without modifying the default k_{max} value

among configurations. The PVC shape parameters determine the steepness of the hydraulic response (c_k) and the range of water potentials at which the plant will start experiencing extreme water stress (Ψ_{p50}). We hypothesized that the RC describes a plant response less affected by low soil water potentials, while the VC describes a plant response with a high susceptibility to hydraulic failure at low water potentials.

The second set of experiments explored the role of k_{max} in constraining the whole plant water use strategy of the different tree species. This was achieved by changing only the k_{max} value of the default configuration (DCk_{max}) to the high (Hk_{max}) and low (Lk_{max}) xylem conductance while keeping the default model configuration for the shape parameters of the vulnerability curve (Table 2). Finally, two additional intermediate values were added to this experiment representing the midpoint between the boundaries and the default k_{max} (1.1 x 10^{-7} mm_{H2O} $mm_{H2O}^{-1}s^{-1}$ and 1.1 x 10^{-8} mm_{H2O} $mm_{H2O}^{-1}s^{-1}$) and are referred to as intermediate-high (IHk_{max}) and intermediate-low (ILk_{max}) xylem conductance, respectively. The optimal choice of the defined k_{max} configurations was selected based on the maximum value of the index of agreement (see section 2.6.4) and is referred to in the manuscript as the 'optimal' k_{max}. For sites where the index of agreement of the 'optimal' k_{max} is lower than 0.6 we used an additional k_{max} configuration corresponding to the midpoint between the best performing k_{max} and the following k_{max} until we achieve an index value > 0.6.

The third set of experiments aimed to evaluate the role of coordinated changes in safety (i.e., shape parameters) and transport capacity (i.e., maximum xylem conductance). We analyzed the plant hydraulic response simulated by CLM5 using the k_{max} configuration that has the largest index of agreement (see section 2.6.4) obtained for each site in the second set of experiments together with both Ψ_{p50} and c_k values used in the first set of experiments (Table 2). We hypothesized that a more appropriate k_{max} value would lead to the expected pattern of vulnerable hydraulic configurations experiencing more water stress. The stress was evaluated based on the variation of the percent loss of conductance (PLC) and the leaf water stress factor (β) described later in section 2.6.3.

2.6. Data Analysis

2.6.1. Reference Evaporation

Equation 5 is based on Equation 6 from Allen et al. (1998), and calculates the reference evaporation (E_o) used as a descriptive variable of the atmospheric water demand for each experimental site but has no relevance for the model simulations. Equation 5 assumed a reference crop of 0.12 m height, a surface resistance of 70 s m^{-1}, and an albedo of 0.23. This equation requires wind speed (u) in m s^{-1}, net radiation (R_n) and ground heat flux (G) both in MJ $m^{-2}d^{-1}$, air temperature (T) in C, and the actual and saturated vapor pressures (e_a and e_s, respectively) in kPa. G was extracted from the modeled results of the default configuration of each experimental site. The slope of the saturation vapor pressure curve at air temperature (Δ, kPa K^{-1}) was computed using Equation 6, based on Equation 13 from Allen et al. (1998). The psychrometric constant (γ) was estimated with Equation 7 based on Equation 8 from Allen et al. (1998), where λ is the latent heat of vaporization (2.45 MJ kg^{-1}), c_p is the specific heat at constant pressure (1.013 x 10^{-3} MJ kg^{-1} K^{-1}), p is the atmospheric pressure (kPa), and ϵ is the molecular weight ratio of water vapor and dry air (0.622).

$$E_o = \frac{0.408 \cdot \Delta \cdot (R_n - G) + \gamma \frac{900}{T + 273} \cdot u \cdot (e_s - e_a)}{\Delta + \gamma \cdot (1 + 0.34 \cdot u)}$$	Equation 5

$$\Delta = \frac{4098 \cdot \left(0.6108 \cdot exp^{\left(\frac{17.27 \cdot T}{T + 273.3}\right)}\right)}{(T + 237.3)^2}$$	Equation 6

$$\gamma = \frac{c_p p}{\epsilon \lambda}$$	Equation 7

2.6.2. Upscaled Transpiration

Observed forest transpiration (E_T) in mm hr^{-1} was calculated based on the hourly and sub-hourly sap flux of individual trees (Q_{tree}) in cm^3 hr^{-1} available on the SAPFLUXNET data set (Poyatos et al., 2020). We used equation 8 to obtain E_T and summarized it in daily time steps following the recommendations of Nelson et al. (2020). Equation 8 requires Q_{tree} aggregated in hourly fluxes per tree (m^3 hr^{-1}tree^{-1}), the basal tree area (Ω_{tree}) in m^2 tree^{-1}, the stand basal area (Ω_{stand}) in m^2 m^{-2}, and the number of measured trees (n). All the information required in Equation 8 is available on the SAPFLUXNET data set for each site. The stand basal area of DE-Hin was missing in the SAPFLUXNET data set, so we obtained it from Moreno et al. (2017) according to the geographical location of the plot.

$$E_T = \frac{\Omega_{stand}}{n \cdot 10^3} \cdot \sum_{tree=1}^{n} \frac{Q_{tree}}{\Omega_{tree}}$$	Equation 8

2.6.3 Plant Water Stress

The plant water stress was evaluated by comparing the percentage loss of hydraulic conductance (PLC) and the transpiration water stress parameter (β). The PLC was calculated using Equation 9 at the root-stem (hereafter named stem) and stem-leaf (hereafter named leaf) plant segments. This equation uses the simulated (k) and the maximum (k_{max}) plant organ conductance, where low PLC values represent a stressed plant segment. The leaf water stress factor (β_x) of each component (i.e., sunlit and shaded leaf) is used to down-regulate the photosynthesis and stomatal conductance (D. M. Lawrence et al., 2019) and ranges from 0 (fully stressed component) to 1 (non-stressed component). The β_x is calculated as the ratio of the actual stomatal conductance ($g_{x.s}$) over the unstressed stomatal conductance ($g_{x.max}$) (Equation 10). The canopy water stress factor (β) is calculated as the weighted average of shade and sunlit components according to their corresponding LAI components (Equation 11). Further details on the mathematical formulation of β factor of CLM5 are provided in Kennedy et al. (2019).

$$PLC = 100 \cdot \left(1 - \frac{k}{k_{max}}\right)$$	Equation 9

$$\beta_{\mathrm{x}} = \frac{g_{\mathrm{x.s}}}{g_{\mathrm{x.max}}}$$	Equation 10

$$\beta = \frac{\beta_{\mathrm{sunlit}} \cdot \mathrm{LAI}_{\mathrm{sunlit}} + \beta_{\mathrm{shaded}} \cdot \mathrm{LAI}_{\mathrm{shaded}}}{\mathrm{LAI}_{\mathrm{sunlit}} + \mathrm{LAI}_{\mathrm{shaded}}}$$	Equation 11

We used the modeled PLC as a proxy of realistic plant responses considering that when the PLC is closer to 12%, the stomatal control of the plants prevents the trees from reducing the internal water storage and dehydrating further. When the PLC is closer to 50% the hydraulic stress in the plants triggers a series of negative effects such as leaf shedding or partial dieback of branches, and the recovery process of the plant does not necessarily reach a full recovery. Meanwhile, when the PLC is closer to 88% it is considered that most of the trees are dying or are already dead (Choat et al., 2018; Johnson et al., 2012; Meinzer et al., 2009; Preisler et al., 2022).

2.6.4 Index of Agreement

The data analysis across sites and model configurations focused on comparing the measured and modeled transpiration during extended summer periods lasting from May to September using the Index of Agreement (Γ) proposed by Duveiller et al., (2016). Equation 11 determines Γ as the product between an α coefficient and the Pearson correlation coefficient (r). The α coefficient represents any bias existing between measured and modeled daily transpiration rates, where a value of 1.0 represents a perfect agreement between both data sets and a 0 value means no agreement between them. This coefficient is determined using the standard deviation of measured and modeled transpiration (σ_X and σ_Y, respectively) and their mean values ($\bar{X}$ and $\bar{Y}$).

$$\Gamma = \alpha \cdot r \quad \text{where } \alpha = f(x) = \begin{cases} 0, & \text{if } r \leq 0 \\ \dfrac{2}{\dfrac{\sigma_X}{\sigma_Y} + \dfrac{\sigma_Y}{\sigma_X} + \dfrac{(\bar{X} - \bar{Y})^2}{\sigma_X \cdot \sigma_Y}}, & \text{otherwise} \end{cases}$$	Equation 12

3. Results

The impact of the different plant hydraulic parametrizations was investigated by comparing the simulated time series of transpiration (E_{Tm}) to the upscaled sap flux measurements (E_{T}). Furthermore, a comprehensive insight into the simulated plant hydraulic response was gained by analyzing the temporal evolution and probability density of PLC, the transpiration water stress parameter (β), and the water potentials across the soil-vegetation continuum (Ψ).

3.1. Reference Evaporation and Measured Transpiration

Figure 3 shows the multiannual variability of E_{o} and E_{T} for each site. During the extended summer period, the atmospheric water demand is two- and four-times larger than the

E_T in FR-Hes/DE-Hin and FR-Pue/ES-Alt, respectively. It is worth noting that despite belonging to the same climate classification, the DE-Hin and FR-Hes sites have a large difference in E_o values. This difference is linked to lower temperatures at DE-Hin compared to FR-Hes. E_T patterns differ among species, with sites dominated by *Fagus sylvatica* (i.e., FR-Hes and DE-Hin) showing maximum E_T values of more than 4 mm d^{-1} during summer and 0 mm d^{-1} in spring and autumn due to the deciduousness of the forest species. In contrast, the evergreen *Quercus ilex* at FR-Pue and ES-Alt keep maximum E_T values lower than 4 mm d^{-1}, have smaller intra-seasonal variations with greater spring and autumn E_T, but smaller values in summer compared to the *Fagus sylvatica* sites.

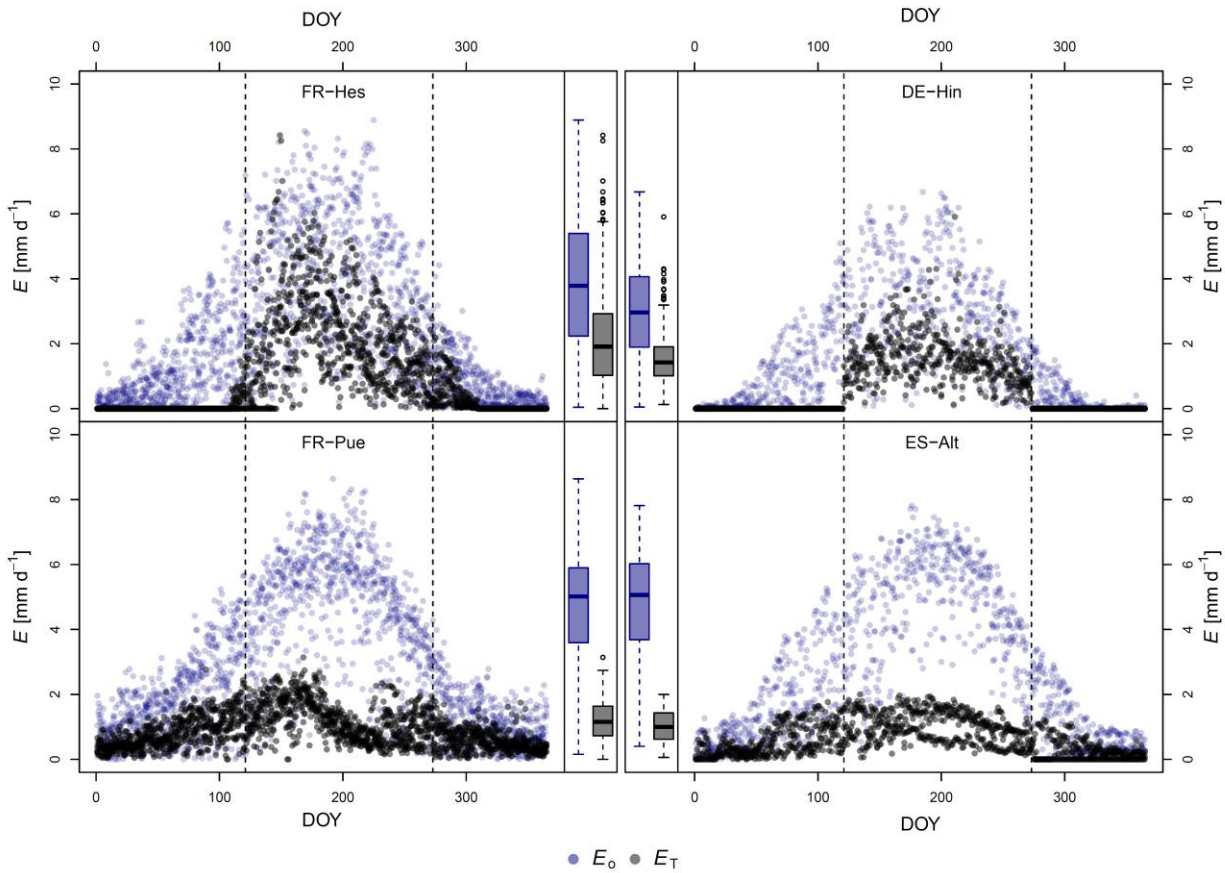

Figure 3. Multi-annual variation of reference evaporation (E_o) and measured daily transpiration (E_T) of the four forested sites in Europe. The dashed vertical lines show the extended summer period (from May to September) used for the current analysis of model results. The box plots show the difference between E_o and E_T of the extended summer period for each site.

3.2. Effects of Changing the Shape of the Vulnerability Curve

Looking first at the deciduous sites, the experimental site FR-Hes has similar measured and modeled transpiration estimates with Γ values larger than 0.7 (Figure 4), with the DC having the best E_T representation. Nonetheless, the data distribution (i.e., interquartile range) of the VC has a better match than the DC with the observed transpiration despite its slightly lower Γ value

(VC: 0.73, DC: 0.76).. The Γ values in DE-Hin are larger than 0.5 with the VC as the best representation of the E_T in this site (Γ= 0.65), with minor differences during the end of the extended summer period (see Figure S1). The RC and DC show a significant over-estimation of E_T during May (see Figure S1). Figure 4 indicates that there are marginal differences of the PLC at the root-stem segment at both sites (i.e., FR-Hes and DE-Hin) when representing a vulnerable (VC) and resistant (RC) shape of the vulnerability curve. As expected, the VC tends to produce lower transpiration rates and higher water stress conditions represented by low β values. These stress conditions are mainly found at the stem-leaf level with the median of the PLC values going beyond 12% while those at the root-stem level remain close to zero. The comparison of the distribution of the PLC values at different plant levels (i.e., root-stem and stem-leaf) with those of the β stress factor provides some additional insights into the relative effect of stomata and plant hydraulics on the simulated transpiration response. For example, the low root-stem values at FR-Hes and DE-Hin show that β is influenced by environmental stressors at leaf level, because there is no strong reduction of the plant hydraulic conductance at the root-stem segment (Figure 4).

The effects of changing the shape of the vulnerability curve are remarkably different at the evergreen sites (i.e., FR-Pue and ES-Alt) populated with *Quercus ilex* species (Figure 4). At these sites, all configurations overestimate the transpiration response in May, which leads to a strong underestimation of E_T during prolonged dry conditions of summer and followed by a slow recovery in September (see Figure S1). Counterintuitively, the resistant configuration (RC) does not alleviate the canopy stress as expected; meanwhile, the vulnerable configuration (VC) simulates higher transpiration rates than the default configuration (DC) during most of the summer. The unexpected model response is confirmed by the distribution of the simulated water stress factor and PLC values, with the response of the RC and VC reflecting a higher level of hydraulic failure compared to DC. The sites FR-Pue and ES-Alt show that β is partly influenced by the reduction of the plant hydraulic conductance for part of the extended summer, because both sites have a large period experiencing low PLC values (PLC < 50%) at the root-stem compartment.

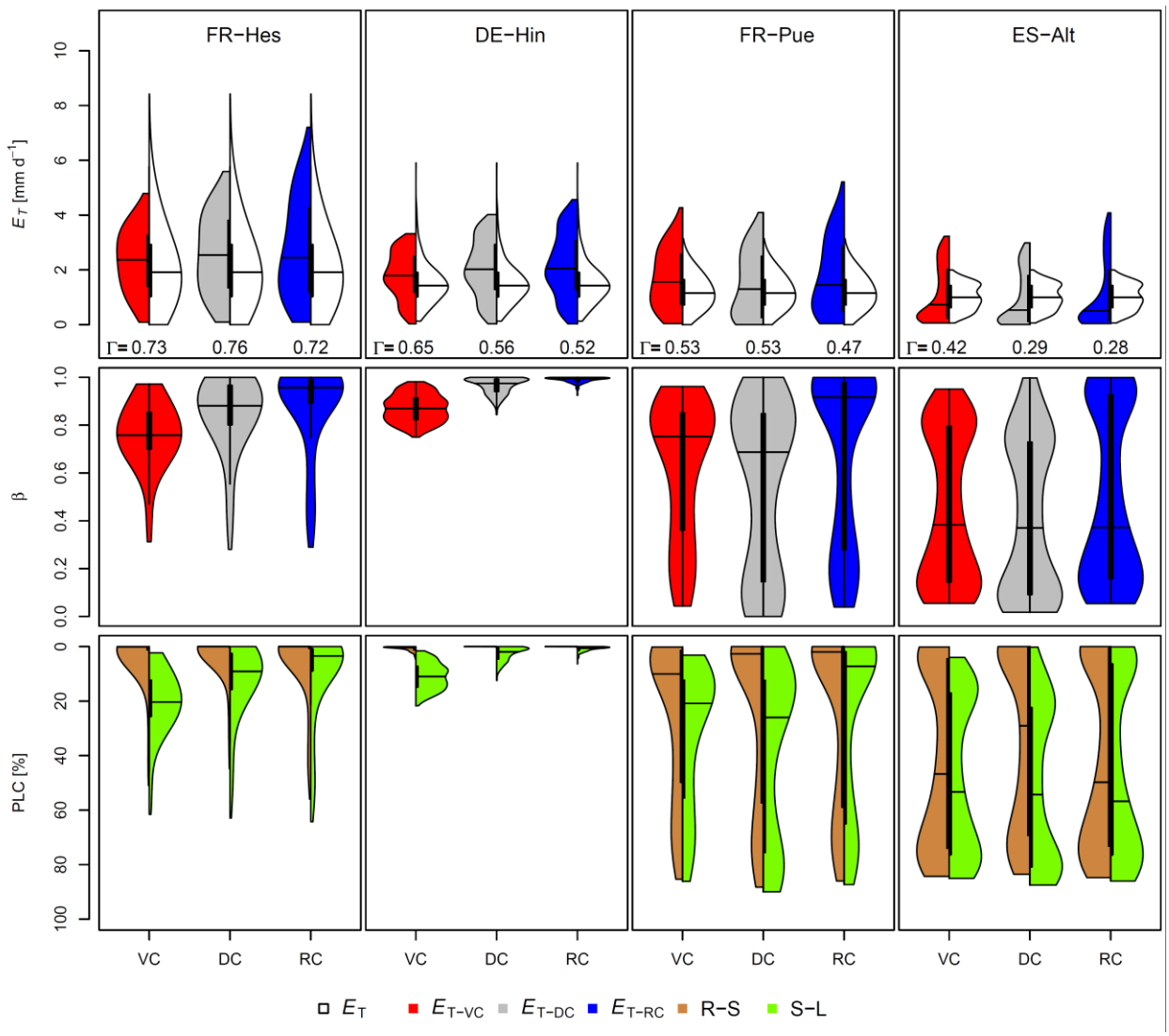

Figure 4. Distributions of daily transpiration (E_T), leaf water stress factor (β) and percentage loss of hydraulic conductance (PLC) during extended summer periods for different hydraulic vulnerability configurations. Each configuration represents a specific combination of the shape parameters (i.e., Ψ_{p50} and c_k) of the plant vulnerability curve. Each violin plot contains the multi-annual data for each site. The distribution of measured E_T is contained in the upper row plots of each site, with the observations shown on the right side of each violin plot (in dark green), and the simulations using the vulnerable (VC), default (DC), and resistant (RC) configurations shown on the left side, in red, grey, and blue, respectively. The PLC values per configuration and site are split between the plant compartments root-stem (R-S) and stem-leaf (S-L) colored in brown and lime green, respectively.

3.3. The Regulating Effects of Xylem Conductance

The second set of numerical experiments investigated the extent to which the water use strategy can be modified in the model through gradual changes over a spectrum of k_{max} values. Figure 5 illustrates how the default k_{max} configuration (DCk_{max}) has the relatively best performance at FR-Hes (Γ=0.818) compared to other sites (Γ<0.7). Also, this figure shows that moving from the high k_{max} (Hk_{max}) towards the low k_{max} (Lk_{max}) configuration, the simulated transpiration can be 'adjusted' to better capture the differences in transpiration seasonality at the four selected sites. The Hk_{max} and intermediate high k_{max} (IHk_{max}) did not show differences in the simulated E_T for the selected sites, as within this range of k_{max} values transpiration rates are limited by the atmospheric water demand. Most effective changes in the simulated E_T values occur in the range between the default k_{max} (DCk_{max}) and low k_{max} (Lk_{max}), with the best correspondence between observed sap flow and simulated transpiration rates achieved by ILk_{max} for all the sites. Here it is interesting to note that at ES-Alt, the model performances can be further improved by increasing the sampled k_{max} values between ILk_{max} and Lk_{max} (see Figure S4), with an 'optimal' k_{max} value of 6.5 x 10^{-8} mm_{H2O} $mm_{H2O}^{-1}s^{-1}$.

We found that gradual changes in k_{max} systematically affected the soil matric potential (Ψ_{soil}) across all sites (Figure S2). This tendency shows the impact of transpiration on the soil water reservoir by increasing the plant water acquisition. Higher k_{max} values allow more water to be extracted from the soil and hence a reduction in the soil moisture. In contrast, reduced k_{max} compared to the default value results in a reduced water transport capacity and diminishing soil water acquisition. The Lk_{max} configuration restricts the plant water transport at all sites to a point where the soil matric potential is close to 0 all year round (Figure S2).

Sites covered with *Fagus sylvatica* do not experience extreme transpiration stress (β<0.5) even when the E_T is overestimated as in the Hk_{max}, IHk_{max}, and DC configurations (Figure 5). The increment of leaf water stress with the Lk_{max} configuration at these two sites (i.e., FR-Hes and DE-Hin) does not go beyond 0.5. This is the result of a constrained water transport within the plant due to the limitation created by an extremely low k_{max}. Therefore, the stomatal conductance used to determine the β values is reduced, increasing the difference between the stomatal conductance (g_s) and the maximum g_s (g_{max}). The sites with *Quercus ilex* (i.e., FR-Pue and ES-Alt) experience a more significant leaf water stress in summer when the k_{max} overestimates the transpiration in spring (Hk_{max}, IHk_{max}, and DC). The use of smaller k_{max} values at these drier sites triggers a more restricted vegetation water use under wet conditions (i.e., spring and early summer). Using a smaller k_{max} at sites with stronger dry seasons enables the vegetation to not use all the water in spring, allowing the soil water reservoir to supply the moisture needed in summer.

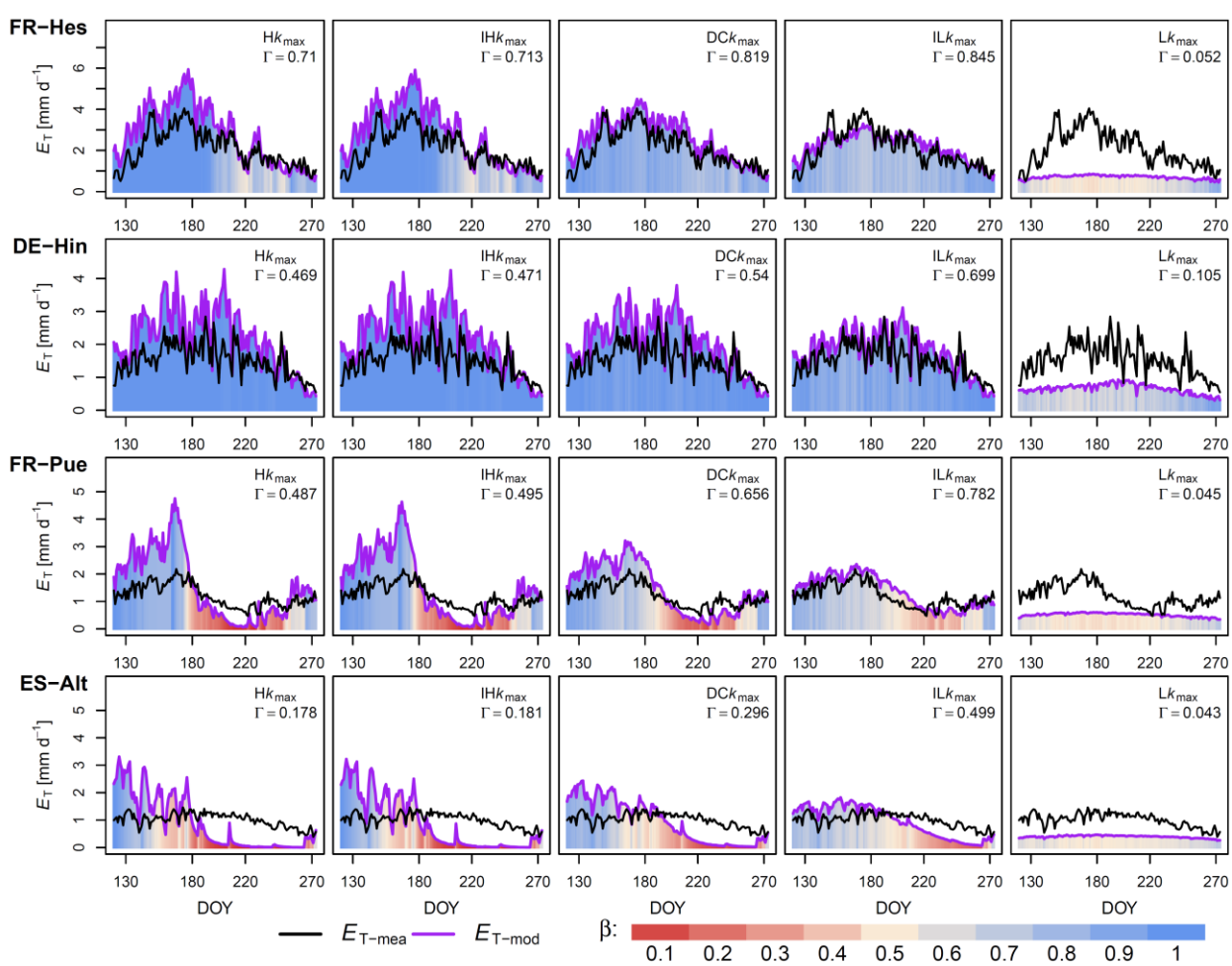

Figure 5. Temporal variation of measured transpiration ($E_{T\text{-mea}}$), modelled transpiration ($E_{T\text{-mod}}$), and leaf water stress factor (β) to gradual changes of maximum xylem conductance (k_{max}) at each experimental site. The plots for each site represent a decrease of maximum xylem conductance from left (larger k_{max}) to right (low k_{max}). The leaf water stress (β) in each plot is represented by daily bars and tends towards reddish colors when β falls below 0.5 (extreme stress), while the blueish colors represent unstressed leaf conditions (β above 0.5). The index of agreement (Γ) is used for comparing the different model configurations per site.

3.4. The Combined Effects of Changing the Shape of the Vulnerability Curve and the Maximum Xylem Conductance

The third set of experiments was designed to evaluate the sensitivity of E_T to the plant vulnerability curve (PVC) parameters with the modified k_{max}. We expect that the use of best-fitted k_{max} values obtained in the second set of experiments allows a better evaluation of the impacts of the coordinated changes between c_k and Ψ_{p50}. As compared to Figure 4, the simulated E_T is much closer to the observed at all sites for DC, also avoiding extreme stress at xylem level (PLC < 50%) for extended periods (Figure 6). Furthermore, the coordinated changes of the shape

parameters with the k_{max} enable the simulation of a more realistic hydraulic response of the root-stem and stem-leaf segment to dry season conditions across the four selected sites (Figure 6). Similarly to the experiment 1, the results indicate that at sites populated by *Fagus sylvatica*, the severe hydraulic failure events (PLC > 50%) simulated by the model are much less frequent at FR-Hes and are completely absent at DE-Hin. Meanwhile, the Mediterranean sites (i.e., FR-Pue and ES-Alt) are characterized by low PLC values (<20 %) for the root-stem plant segment, while more severe PLC values are simulated at the stem-leaf level. Only the RC of these evergreen sites shows a more severe stress response in summer, where the root-stem compartment experiences PLC values larger than 20% for half of the time (second half of the violin plot of Figure 6). At the same time, the xylem-leaf compartment also shows a strong reduction of conductance (PLC > 50%). The impact of the RC also affects the xylem-leaf compartment, where the bimodal distribution depicts the problem of the reduced provision of water for vegetation during summer due to a more aggressive soil water extraction in late spring or early summer.

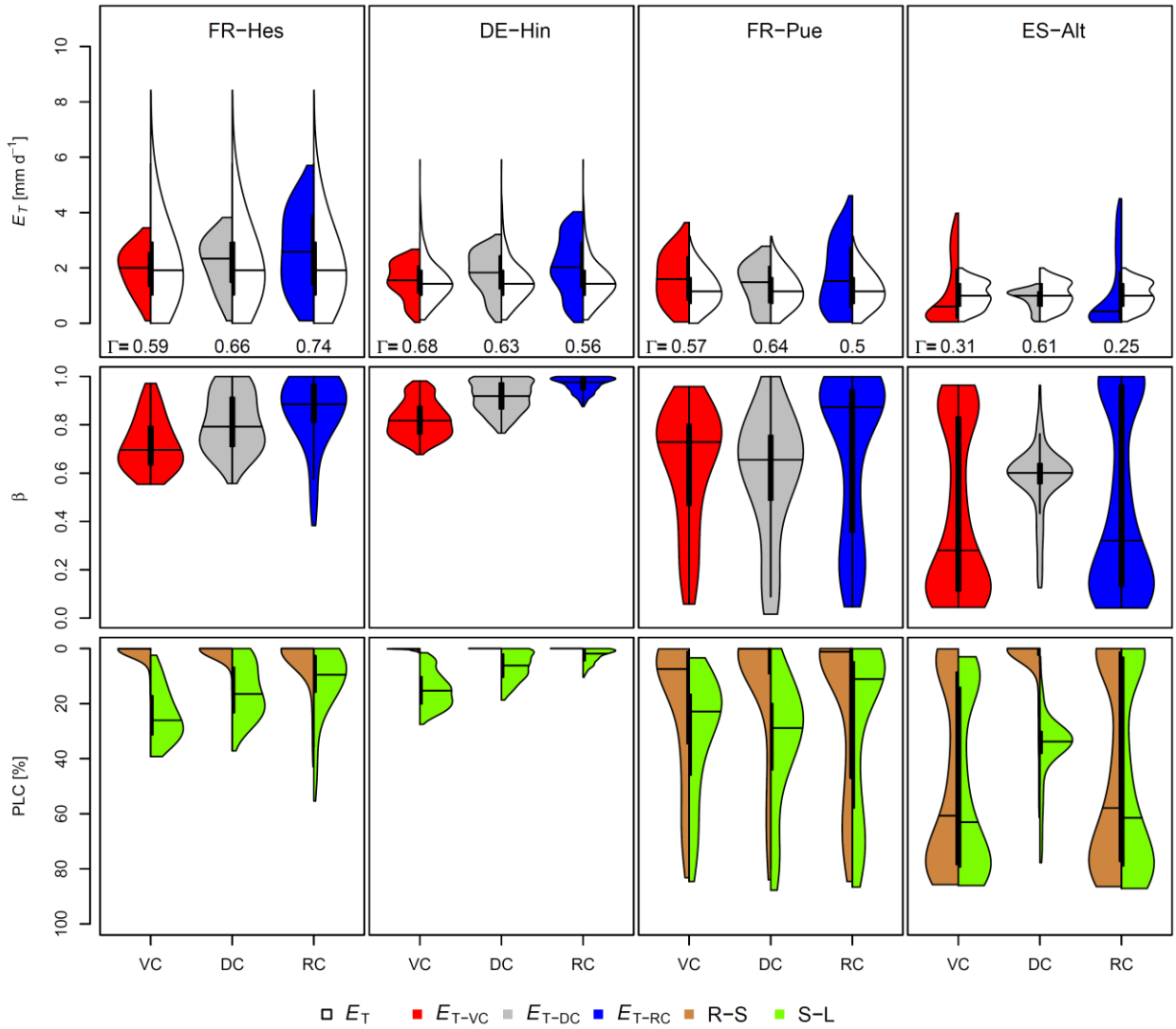

Figure 6. Distributions of daily transpiration (E_T), leaf water stress factor (β) and percent loss of conductance (PLC) during the extended summer period for different hydraulic vulnerability configurations with optimal k_{max}. Each configuration represents the specific combination of the shape parameters (i.e., Ψ_{p50} and c_k) of the plant vulnerability curve and the optimum k_{max} per site from Experiment 2. Each violin plot contains the multiannual data for each site. The distribution of measured E_T is contained in the upper plot of each site (solid dark green). The vulnerable (VC), default (DC), and resistant (RC) configurations are represented by red, grey, and blue solid colors, respectively. The PLC values per configuration and site are split between the plant compartments root-stem (R-S) and stem-leaf (S-L) colored in brown and lime green, respectively.

4. Discussion

4.1. What is known about the selected tree species?

Fagus sylvatica and *Quercus ilex* are two tree species with contrasting responses to dry periods. These responses depend on physiological adaptations and the cumulative exposure to specific environmental conditions that shape the WUS of each species. *Fagus sylvatica* relies on a small water reservoir because of its shallow root system (Houston Durrant et al., 2016; Kirchen et al., 2017; Leuschner, 2020). This has been documented at FR-Hes and DE-Hin (Granier et al., 2000; Heinrich et al., 2018), where the species were found to be more susceptible to reductions of soil water availability due to dry spells and droughts. This tree species prefers to grow in environments with abundant precipitation, with no water stagnation on the ground or prolonged dry periods (Houston Durrant et al., 2016; von Wuehlisch, 2008). This could be why *Fagus sylvatica*, keeps significant transpiration rates as leaf water potentials decline, but it is also frequently observed to shed leaves prematurely under extreme drought, which could be due to reduce water loss and hydraulic failure or due to hydraulic failure (Leuschner, 2020).

Quercus ilex can grow deep roots, increasing the accessible water reservoir and allowing the trees to withstand long dry periods (Peñuelas & Filella, 2003; Zapater et al., 2011), as has been shown at FR-Pue and ES-Alt (Baldocchi et al., 2010; Forner et al., 2018). Its evergreen character is maintained during summer thanks to its physiological adaptations such as sclerophyllous leaves, summer growth reduction, and strong stomatal control (Barbeta & Peñuelas, 2016; Terradas & Savé, 1992). The high wood density of oak is linked to its reduced porosity, allowing it to resist lower matric potentials during summer, reducing its susceptibility to hydraulic failure (Terradas & Savé, 1992). The strong stomatal control of this species classifies it as the most isohydric species of the *Quercus* genus (Barbeta & Peñuelas, 2016). This process is clearly visible in summer at FR-Pue and ES-Alt, where precipitation is scarce, and the trees reduce transpiration rates by closing their stomata. Overall, the difference between the two selected species relies on the degree of vulnerability to hydraulic failure and the WUS, with *Fagus sylvatica* showing a vulnerable response and aggressive WUS, while *Quercus ilex* is more resistant to hydraulic failure with a conservative WUS.

4.2. Some unexpected effects of the vulnerability curve shape parameters

The plant vulnerability curve (PVC) is widely used to model the plant water use response to water stress from single trees up to the ecosystem scales (Kennedy et al., 2019; Li et al., 2021; Mackay et al., 2015; Mencuccini et al., 2019; Sloan et al., 2021). However, linking a PVC to a vegetation classification framework based on plant form and phenology, such as the PFT system,

introduces biases linked to the homogenization of highly diverse plant responses (Matheny et al., 2017). Despite the existence of some species-specific LSM studies focused on the impact of varying the PVC parameterizations for different species within the same PFT (e.g., De Kauwe et al., 2022; Sabot et al., 2020), to our knowledge, the impact of characterizing the shape parameters of the PVC (Ψ_{p50} and c_k) for the same species or plant functional types (PFTs) has not been investigated in detail for the current implementations of the PVC in land surface models (LSMs). In CLM5, the default parameterization of the plant hydraulic traits is the same for the PFTs under analysis at the four experimental sites. This parameterization does not agree with the current evidence showing a high degree of variability for parameters such as Ψ_{p50} (e.g., Eller et al., 2020; Lu et al., 2022; Xie et al., 2023). Nonetheless, this homogeneity in the parameterization of the plant hydraulic traits of CLM5 provided the opportunity to evaluate the effect of the environmental conditions, namely the dynamics of atmospheric water demand and soil water availability, on the simulated plant hydraulic response. FR-Hes and DE-Hin are sites with a continuous water supply during summer due to the low intra-seasonal variability of precipitation (Blume et al., 2022; Granier et al., 2008). Regular precipitation prevents the drying out of the soil water reservoir during summer, allowing the vegetation to operate at low to moderate levels of water stress throughout the year. The default plant hydraulic parameterization of CLM5 reproduces an aggressive water use strategy (WUS) of *Fagus sylvatica* at FR-Hes, allowing the vegetation to transpire at rates close to the atmospheric water demand. However, the use of the same plant hydraulic parameterization across the selected PFTs (Table 2) does not reflect the conservative WUS expected at Mediterranean sites, such as FR-Pue and ES-Alt, which are inhabited by *Quercus ilex*. These two sites have a strong atmospheric water demand but receive very little precipitation in summer (Allard et al., 2008; Lorenzo-Lacruz et al., 2010), resulting in extremely negative soil water potentials and severe plant water stress in the default model simulations (Jiménez-Rodríguez et al., 2022). Although, the inclusion of water uptake from deeper soil reservoirs can also reduce the severity of simulated water stress and under-estimation of transpiration rates in the model during summer periods, as shown by Jiménez-Rodríguez et al. (2022), the need to regulate the extreme plant water consumption during un-stressed wet periods prevailed.

The limitations underscored by the default plant hydraulic parameterization of CLM5 in reproducing the aggressive and conservative WUS persist when changes are applied only to the Ψ_{p50} and c_k parameters. That is, the model response is dominated by the instantaneous atmospheric water demand and restricted by the soil water availability. Therefore, at sites where water supply is continuous throughout the year (e.g., FR-Hes and DE-Hin) the decrease of Ψ_{p50} with the resistant configuration (RC) allows more water to be extracted under given meteorological conditions while reducing plant water stress (PLC and β) as expected (Knüver et al., 2022; Walthert et al., 2021). However, the deciduous character of both sites with leaf absence during the first part of the year does not prevent the RC configuration from overestimating transpiration rates (E_T) for both sites (Figure 4 and Figure S1) during the first part of the extended summer. This pattern of the model response illustrates the dominant role of plant hydraulics over stomatal control of E_T. Under seasonally limited soil water supply, as is the case at FR-Pue and ES-Alt during summer, the model simulates a counter-intuitive response when changing the shape parameters of the PVC, with the resistant configuration (RC) suffering more water stress and a reduced E_T than the default or vulnerable configurations (DC and VC, respectively) (Figure 4). The entire intraspecific variability in PVC shape parameters for *Quercus ilex* does not reproduce the conservative WUS in the model that would be expected of a

tree species able to withstand significant water shortage conditions (Barbeta & Peñuelas, 2016; Terradas & Savé, 1992). On the contrary, the choice of more resistant PVC shape parameters diminished the soil water availability simulated at FR-Pue and ES-Alt during summer due to over-use of water in spring, magnifying the overall vegetation water stress.

4.3. Uncovering the role of maximum xylem conductance

The results of the second set of numerical experiments highlight the role of the maximum xylem conductance (k_{max}) in determining the transpiration rates under ample water supply and therefore shaping the seasonal water use strategy. Here we found that reducing the plant hydraulic conductance can improve both, the over-estimation of transpiration in the early growing season and the under-estimation in late summer, due to more carry-over soil resources from the early to the late season. These results illustrate the effective role of k_{max} in constraining the water use at sites with seasonal water limitations (i.e., FR-Pue and ES-Alt). The maximum hydraulic conductance is a parameter highly influenced by plant segment age (Weithmann et al., 2022) and local environmental conditions rather than genetics (Hochberg et al., 2018; Lu et al., 2022). However, the complex interactions between environmental conditions and individual species made it difficult to identify individual environmental drivers for temperate tree species such as *Acer platanoides* L., *Carpinus betulus* L., and *Tilia cordata* Mill (Fuchs et al., 2021). The response of species response of hydraulic conductance to contrasting soil conditions is not fixed among species where *Fraxinus ornus* L. had shown a strong sensitivity to soil dryness (Gortan et al., 2009) while other species such as *Pinus sylvestris* are not affected by such soil gradients (Jackson et al., 1995). The high environmental plasticity has been documented for *Fagus sylvatica* (Weithmann et al., 2022) pointing out the age of the plant segments as the principal driver defining the hydraulic conductance. This characteristic is represented by the range of k_{max} values observed for *Fagus sylvatica* and *Quercus ilex* (Figure S5). The observed k_{max} values vary by two orders of magnitude for *Fagus sylvatica* (BDT) and five orders of magnitude for *Quercus ilex* (BET), with similar maximum values for both.

The primary role of k_{max} for the plant hydraulic system of CLM5 is in constraining the water transport during unstressed conditions and thereby determining the magnitude of plant water use and how much water is left in the ground, some of which might be available later. At FR-Hes, larger k_{max} values compared to the default value increase the water transport in the model, allowing to match the atmospheric water demand and transpiration measurements. In contrast, smaller k_{max} values are needed at ES-Alt and FR-Pue to prevent the vegetation from depleting the soil water reservoir in spring and therefore enable continued plant water use under moderate stress during the dry summer. A lower k_{max} depicts a transport limitation allowing to reduce the water stress on the plant in the model, while a larger k_{max} allows the model to transpire at higher rates, mimicking an aggressive WUS. The large influence that k_{max} has in controlling the water acquisition in CLM5, despite the use of the Medlyn slope for controlling the stomatal conductance, makes the model to work differently than other numerical models that rely on stomatal conductance to control or mimic the WUS (Sloan et al., 2021). Therefore, in CLM5, an adequate selection of k_{max} plays the role of restraining the vegetation from transpiring excessively in spring and at the beginning of summer to ensure an adequate water supply as summer progresses in a Mediterranean (summer-dry) climate. Note that in the Darcy's law equation used in the plant hydraulics system of CLM5 a certain sensitivity in the simulated transpiration fluxes could be expected by also changing the cross-sectional area of the different plant segments (e.g., SAI). However, there is no direct correspondence between the prescribed

SAI values in the model (defined as the sum of all non-photosynthetic vegetation, including stems, branches, and dead leaves (P. J. Lawrence & Chase, 2007)) and the basal area reported from the selected sites (Table 1). Therefore, the uncertainty added using this variable in the simulated transpiration fluxes cannot be explained by structural properties of the forest.

Most models describe the plant vascular factor by lumping the entire system into a single term (Fatichi et al., 2016), omitting the large variability of the forest ecosystems related to tree species and age (Weithmann et al., 2022). This is the case for k_{max} that is a key plant hydraulic trait contributing to the control of the water transport capacity of vegetation (Eamus et al., 2016). Within the plant hydraulic system of CLM5 the default k_{max} value is commonly used, disregarding the variability of different tree species and stand density within the PFT classification. This plant hydraulic trait (PHT) varies accordingly with the plant species, environmental conditions, and tree size (Anfodillo & Olson, 2021; Domec et al., 2012; Domec Jean-Christophe et al., 2008; Hochberg et al., 2018; Willigen et al., 2000), but previous studies argued that k_{max} expresses the maximum xylem conductance of vegetation under the most favorable environmental conditions (Sabot et al., 2020). However, to link k_{max} with the experimental evidence based on measurements of specific xylem conductance (k_s) it is necessary to include the forest structure (e.g., forest height, branch network) to upscale and better represent the water flux within the vegetation.

The use of plant hydraulics in land surface modelling provides a framework to connect the water stress with the stomatal response (Venturas et al., 2017), allowing a better control on the simulated plant water use strategies. However, the site-specific character of k_{max} has largely been ignored by the modelling community. In CLM5, the default value for k_{max} is the same for all PFTs, and an order of magnitude lower than the lowest reported specific xylem conductance (k_s) for *Fagus sylvatica*, whereas the reported values for *Quercus ilex* have two outliers, one and three orders of magnitude below the default value (see Figure S5 for more details). The k_s values of *Fagus sylvatica* do not match the range of k_{max} used in the second experiment, where the high xylem conductance (Hk_{max}) is close to the lowest k_s value found for this tree species. However, we found little difference in the simulations between the highest values of k_{max}, so exploring the range of values where most observations lie would not improve the model simulations. The differences between the reported k_s and model-default k_{max} highlights the complexity of defining the k_{max} value for different plant functional types (PFTs) based on experimental data with a larger number of species. The lack of detailed experimental k_s data of tree roots for different tree species increases the difficulty to better understand the impact of the interaction between soil type and whole plant k_{max}. The data availability constraint also extends to the continuous monitoring of water potentials across and within ecosystems (Novick et al., 2022). There are some studies providing discrete measurements of soil water potential (e.g., Zapater et al., 2011) and predawn leaf water potentials (e.g., Lavoir et al., 2009; Peiffer et al., 2014) for the selected study sites. However, the scarcity of continuous data sets does not allow the analysis of the most stressful period during the day (i.e., noon) or the cumulative effect of water stress in the soil-plant-atmosphere continuum. Nonetheless, the few data available for FR-Pue (i.e., Lavoir et al., 2009) show a range changing from -1 MPa in early spring (i.e., DOY=90) to -5 MPa during the peak of summer (i.e., DOY= 250). This range of predawn leaf water potentials agrees with the leaf water potentials reproduced by the model during the same year and period (see Figure S7). Here we show how important the correct parametrization of k_{max} is in CLM5 for capturing the water use by vegetation in summer-dry climates. To progress, we need a better understanding of

how k_{max} is controlled by a complex set of growing conditions and co-ordination between the root system and leaf area index (Aranda et al., 2015; Lemoine, Jacquemin, et al., 2002).

4.4. Understanding the impact of coordinated changes of plant hydraulic traits in CLM5

We found that the adjustment of the hydraulic vulnerability curve shape parameters (Ψ_{p50} and c_k) alone did not enable the reproduction of the observed water use dynamics (Figure 4), as choosing a parameterization that is more resistant to hydraulic failure (RC) resulted in even more reduced dry season water use, if the maximum hydraulic conductance (k_{max}) was too high. Indeed, the drastic effect caused by the more negative Ψ_{p50} of the RC is diminished by using a smaller k_{max}, reducing the water extraction in spring, and letting the vegetation experience lower PLC values in summer (Figure 6). Also, the fact that the VC of *Fagus sylvatica* results in low PLC for the root-stem and more severe PLC for stem-leaf shows the model's ability to reproduce important physiological processes along the PLC curve (Huber et al., 2019). These processes may trigger different drought survival strategies depending on the species. For *Fagus sylvatica*, water stress and loss in conductance may result in premature shedding of leaves during dry conditions (Arend et al., 2022) or stomatal closure (Schuldt et al., 2016). The sites populated by *Quercus ilex* are better simulated using low k_{max} values (Figures 5 and S4), which allow to better reproduce the WUS of species adapted to water scarce environments (Terradas & Savé, 1992). Nonetheless, extremely low Ψ_{p50} still trigger an excessive water uptake during the driest part of the summer at Mediterranean sites (Figure 6), demonstrating the lack of stomatal regulation in the model and its strong dependency on hydraulic limitations and soil water availability to control the magnitude of E_T. Note that in our study, k_{max} was selected based on the default vulnerability curve shape parameters, whereas the latter were adjusted in a second step, using the previously selected k_{max}. The results could likely be improved by choosing an optimal combination of k_{max}, Ψ_{p50} and c_k, but model calibration is not the goal of the present study. Additionally, the fact that CLM5 does not consider the vegetation capacitance increases the need to make use of the differentiation of k_{max} between plant segments, e.g. following the hydraulic vulnerability segmentation hypothesis (Tyree & Ewers, 1991). This hypothesis proposes that the stem should be the most resistant section of the tree, while the distal portions (i.e., roots and leaves) should be the most vulnerable. However, the response of plant segmentation cannot be generalized to all plant species because the effects of segmentation depends on the safety modulation of other plant traits (Wilkening et al., 2023). Our study does not evaluate the effect of different configurations per plant segment due to the lack of experimental data collected using a consistent methodology across plant segments and tree species. Nonetheless, we expect that any hydraulic differentiation between plant segments would lead to strong differences in the plant water stress experienced at the root-stem segment.

The results of our study also demonstrate that generalizing the use of k_{max} as a homogeneous parameter across PFTs in CLM5 prevents an adequate reproduction of the magnitude and timing of E_T at sites in different climates. The fact that the same species (e.g., *Quercus ilex*) is not represented by the same k_{max} at different sites points out that xylem conductance can be influenced by factors other than genetics (e.g., environmental conditions, growth history). Also, the independence between stomatal control and hydraulic conductance in the model is contradictory to what the existing evidence suggests (Franks, 2004). These aspects magnify the effect that more negative Ψ_{p50} has on the water extraction when we change only the curve shape parameters, something that was overlooked in previous studies (e.g., Bai et al. (2021), Song et al. (2020)). The results of the coordinated changes in safety (i.e., the shape

parameters Ψ_{p50} and c_k) and efficiency (i.e., k_{max}) hydraulic traits underline how k_{max} rules the WUS in the model, while Ψ_{p50} and c_k modulate the level of the hydraulic stress experienced. An adequate parameterization of k_{max}, Ψ_{p50} and c_k in combination is critical for obtaining a simulated plant hydraulic response that conforms with the plant water supply theory and the expected physiological response of vegetation subjected to dry conditions. In addition, any issue linked to plant hydraulic parameterization will also affect other variables such as carbon assimilation, forest growth, or tree mortality, which depend on the plant water use by the forest and are highly sensitive to extreme dry conditions (e.g., Joetzjer et al., 2022; Yao et al., 2022).

4.5. Addressing the plant hydraulic traits: homogeneity versus diversity

The plant functional type (PFT) classification system has been a valuable tool for understanding drought resilience from an ecosystem perspective (Sturm et al., 2022). However, the large variation in ecosystem functional properties related to the water cycle is insufficiently explained by this classification system (Reichstein et al., 2014). Skelton et al. (2015) stressed the need to characterize the plant response to drought by merging the current knowledge of the water use strategies (WUS) with the xylem vulnerability. To fulfill this need, this classification system requires the characterization of the physiological traits per vegetation type and growing stage. Recent studies have shown the importance of individual tree characteristics (e.g., size, age) that influence the tree water transport capacity (e.g., Bittencourt et al., 2023; Schoppach et al., 2021). The combination of tree growth and environmental condition influence the overall plant hydraulic performance (Fichtler & Worbes, 2012), which could explain the noted differences between sites sharing the same species. The bias introduced by the heterogeneity within individual tree species is enlarged by grouping per vegetation type, because the tree species composition is a major driver when determining the transpiration of different vegetation types (Bachofen et al., 2023). Nonetheless, these aspects are heavily homogenized using the current PFT classification system, affecting the capacity to correctly predict the ecosystem water use (Konings & Gentine, 2017) and leading to a poor predictive skill of the vulnerability to hydraulic failure (Matheny et al., 2017).

Fagus sylvatica and *Quercus ilex* represent part of the variability of the plant hydraulic traits (PHT) within the broadleaf deciduous (BDT) and broadleaf evergreen (BET) PFT classes. Aiming to provide a broader context of the role of homogeneity versus diversity in plant hydraulic trait studies, we sampled the XFT database (Choat et al., 2012) for a preselected set of species per PFT in Europe (Buras & Menzel, 2019a; Fyllas et al., 2020; Leuschner & Meier, 2018) with the emphasis placed on the temperate BDT, BET, and adding the needleleaf evergreen (NET) PFT to enrich the analysis (see Table S2 for details of the sampled species). Figure 7 illustrates that the Ψ_{p50} used by default in CLM5 fails to capture the values of Ψ_{p50} for NET and BDT in Europe, as the default values are not even close to the median values of the distributions. The Ψ_{p50} of NET in CLM5 is way beyond the Ψ_{p88} for this PFT, representing an extremely resistant tree with respect to the published data, while the Ψ_{p50} of BDT depicts a more vulnerable tree closer to the reported median of Ψ_{p12}. The default Ψ_{p50} of BET in CLM5 matches the median of the published data, but the large range showed by this PFT (-0.5 MPa to -9 MPa) raises the question of how much of this variability is driven by geography or environmental conditions. An even more important aspect to be considered is an adequate selection of k_{max} for the PFTs, where the large variability showed for individual species does not agree with the best fitted k_{max} of the model. This finding depicts the issue of considering k_{max} as constant among PFTs when the variability of the species describing these PFTs is large (see Figure S5).

Liu et al. (2020) showed the benefit of including plant hydraulics in Earth System Models improving the modeled vegetation response to climatic drivers, where the overestimation of vegetation water use is a common issue when compared against the traditional processes relying on soil moisture and VPD alone. They also recognize the ability of plant hydraulics to predict vulnerability to droughts. In this regard, Kennedy et al. (2019) did the same for LSMs by introducing the plant water stress routine in CLM5 that compartmentalized the PHT according to PFT type. From an ecosystem perspective, simplifying hydraulic traits into single plant functional types has additional repercussions. Matheny (2021) highlighted the importance of incorporating flexible traits based on prevalent environmental stressors since tree species' sensitivity to water stress is determined by their plasticity to the environment (Haberstroh & Werner, 2022). This plasticity is exemplified by the different k_{max} values in *Fagus sylvatica* and *Quercus ilex* in this manuscript, and the reported variability of xylem specific conductance reported across many orders of magnitude for each species (e.g., Bär et al., 2018; Carevic et al., 2014; Charra-Vaskou et al., 2012; Choat et al., 2012; David et al., 2007; Limousin et al., 2010; Lübbe et al., 2022; Martínez-Vilalta et al., 2002; Tomasella et al., 2019). Flexible traits based on the environmental stressors in CLM5 can be used by the spectrum of PVCs per PFT and exploiting the role of k_{max} in regulating the WUS in the model. By adjusting the k_{max} to better represent the transpiration response we may be able to identify the timing of important physiological processes (e.g., leaf shedding) that differ between the VC and RC. In this way, we may be able to better understand the significant changes in different ecosystem processes triggered by intense dry periods (Oddi et al., 2022).

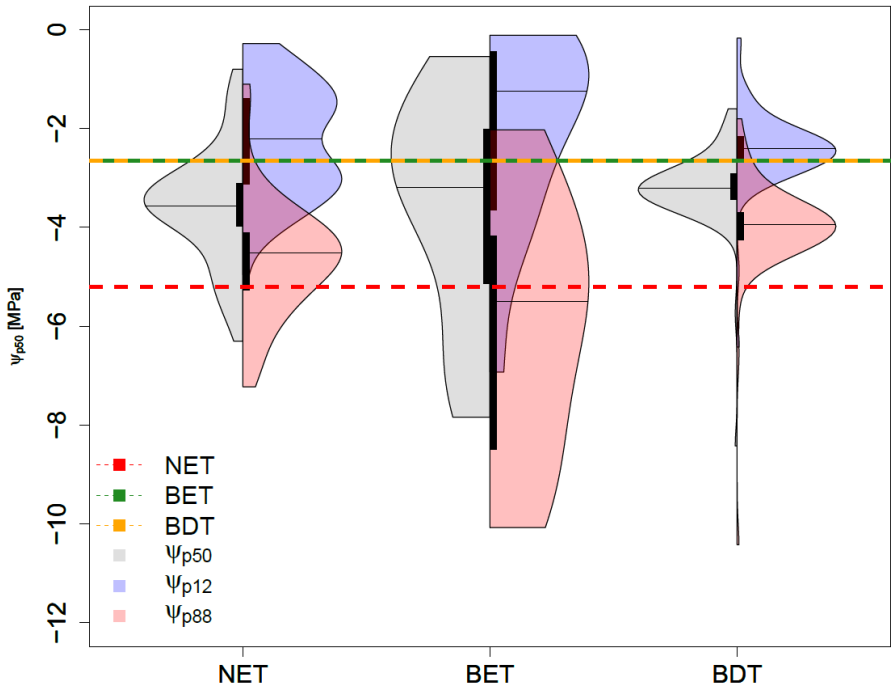

Figure 7. Violin plots describing the variability of the plant hydraulic traits (Ψ_{p12}, Ψ_{p50}, and Ψ_{p88}) within broadleaf evergreen (BET), broadleaf deciduous (BDT), and needleleaf evergreen (NET) trees plant functional types (PFTs) representative of European forests (see Table S2 for the list of pre-selected tree species per PFT). The red, green, and yellow dashed lines represent the NET, BET, and BDT default values of Ψ_{p50} used by CLM5, respectively.

Grouping different tree species into the same PFTs in disregard of their physiological adaptations may affect other parameters that also influence the plant water use within the model. For example, CLM5 calculates the stomatal conductance (g_s) using the Medlyn model (Medlyn et al., 2011). This model uses the minimum stomatal conductance (g_o) that is set to 100 μmol $m^{-2}s^{-1}$ in CLM5 (D. M. Lawrence et al., 2019) and a parameter that links stomatal conductance to photosynthesis (g_1). These two parameters are segregated by PFT in CLM5 according to De Kauwe et al. (2015). However, the g_1 values in the PFT parameterization can deviate greatly from the species specific values reported by Lin et al. (2015). CLM5 uses a g_1 of 4.12 for the broadleaf evergreen trees, which is much larger than the value of 1.73 reported for *Quercus ilex*. This difference may induce an unconstrained transpiration at leaf level when using the default configuration, compromising the coordination of root-stem-leaf conductance. Nonetheless, a lower g_1 value will induce a more constrained transpiration affecting the vegetation capacity to fulfill the atmospheric water requirements (see Figure S6). For the broadleaf deciduous sites (i.e., FR-Hes and DE-Hin), the differences are less pronounced, with the default g_1 value (4.45) being closer to the reported value of 3.24 for *Fagus sylvatica* (Lin et al., 2015). This could be the reason why E_T is over-estimated during wet conditions by the DC at FR-Pue and ES-Alt, but not so much at FR-Hes and DE-Hin (Figure 5)

The use of PFTs in land surface modeling became a cornerstone enabling the reduction of computing time and degrees of freedom thanks to the grouping of species based on plant form and phenology (Colin Prentice et al., 1993). However, this grouping does not respect the large variety in eco-physiological traits within a PFT, leading to strong misrepresentation of some species. Therefore, a better approach for land surface modelling should target the description of the vegetation according to their plant response similarities to CO_2 concentrations and temperatures (Wullschleger et al., 2014), shared evolutionary and optimality principles (Franklin et al., 2020), or by refining the current PFT classification based on key physiological processes that determine the tree response to environmental conditions.

5 Conclusions

The intraspecific variability of the plant hydraulic traits of individual plant functional types (PFT) allows to describe the spectrum of vulnerability to hydraulic failure from vulnerable to resistant responses of different tree species. Understanding the importance of the right selection of k_{max}, Ψ_{p50} and c_k from their large within-species variation requires a detailed understanding of the role played within the model. This information is crucial for the modelling community, where the parameter selection may induce considerable bias when assuming that all tree species within the same PFT behave equally in different environmental conditions. The adequate identification of dominant tree species per experimental site allows to narrow down the variability of multiple species or by weighing the tree species contribution within the PFT but,

given the large variability in hydraulic traits even within a single species, a large uncertainty prevails. Adjustments of the shape parameters of the hydraulic vulnerability curve (Ψ_{p50} and c_k) alone do not enable the model to reproduce E_T during early summer at sites with seasonal water deficits. The seasonal differences between measured and modelled transpiration illustrate the importance of the maximum plant hydraulic conductance (k_{max}) for controlling the magnitude and timing of E_T, i.e. the general water use strategy (WUS). A larger k_{max} allows the trees to transpire larger amounts of water during favorable water conditions, quickly depleting the soil water reservoir. In contrast, smaller k_{max} values limit the water transport and hence soil water extraction rates, pushing the vegetation towards a more conservative WUS. Consequently, k_{max} is a significant player in controlling the transpiration in CLM5 and allowing to mimic the WUS of different species by limiting or enhancing the water transport. However, given the large within-species variability in k_{max}, more research is needed to enable adequate parameterization of the site-specific k_{max}. This work reveals the potential of plant hydraulic traits to mimic aggressive or conservative WUS in CLM5, crucial for adequate reproduction of plant water use dynamics in different climates. Given the large intraspecific variation in plant hydraulic traits and the importance of the stand characteristics (e.g., tree height, stem area index) for limiting transpiration rates in the model, a more fundamental understanding of the drivers for adjustments in these parameters is needed.

Acknowledgments

This work is supported by the Luxembourg National Research Fund (FNR) CORE program (grant no. C19/SR/13652816/CAPACITY). The authors would like to thank Manon Sabot, Simon Jones, two anonymous reviewers, and the Editorial Board for their constructive criticism.

Open Research

The SAPFLUXNET data used for atmospheric forcing and transpiration estimates in the study are available at ZENODO repository via https://doi.org/10.5281/zenodo.3971689 (Poyatos et al., 2020) with a Creative Commons Attribution 4.0 International license for the files. The COSMO-REA6 data used to complete the missing data for the atmospheric forcing in the study are available from the opendata-FTP server at DWD (https://opendata.dwd.de/climate_environment/REA/COSMO_REA6/) (COSMO-REA6, 2019). CLM5.0 is publicly available through the Community Terrestrial System Model (CTSM) git repository (Tag name: release-clm5.0.34) via https://github.com/ESCOMP/ctsm (CTSM, 2017/2022). The results of the numerical experiments, parameter files, and R scripts used during the main data analysis of this manuscript are available at ZENODO repository via https://doi.org/10.5281/zenodo.8019682 with a Creative Commons Attribution 4.0 International license for the files (Jiménez-Rodríguez, 2023).

References

Allard, V., Ourcival, J. M., Rambal, S., Jofre, R., & Rocheteau, A. (2008). Seasonal and annual variation of carbon exchange in an evergreen Mediterranean forest in southern France. Global Change Biology, 14(4), 714–725. https://doi.org/10.1111/j.1365-2486.2008.01539.x

Allen, R. G., Pereira, L. S., Raes, D., & Smith, M. (1998). Crop evapotranspiration-Guidelines for computing crop water requirements-FAO Irrigation and drainage paper 56. FAO - Food and Agriculture Organization of the United Nations.

An, N., Hemmati, S., & Cui, Y.-J. (2017). Assessment of the methods for determining net radiation at different time-scales of meteorological variables. Journal of Rock Mechanics and Geotechnical Engineering, 9(2), 239–246. https://doi.org/10.1016/j.jrmge.2016.10.004

Anfodillo, T., & Olson, M. E. (2021). Tree Mortality: Testing the Link Between Drought, Embolism Vulnerability, and Xylem Conduit Diameter Remains a Priority. Frontiers in Forests and Global Change, 4. https://www.frontiersin.org/articles/10.3389/ffgc.2021.704670

Aranda, I., Cano, F. J., Gascó, A., Cochard, H., Nardini, A., Mancha, J. A., López, R., & Sánchez-Gómez, D. (2015). Variation in photosynthetic performance and hydraulic architecture across European beech (Fagus sylvatica L.) populations supports the case for local adaptation to water stress. Tree Physiology, 35(1), 34–46. https://doi.org/10.1093/treephys/tpu101

Arend, M., Link, R. M., Zahnd, C., Hoch, G., Schuldt, B., & Kahmen, A. (2022). Lack of hydraulic recovery as a cause of post-drought foliage reduction and canopy decline in European beech. New Phytologist, 234(4), 1195–1205. https://doi.org/10.1111/nph.18065

Bachofen, C., Poyatos, R., Flo, V., Martínez-Vilalta, J., Mencuccini, M., Granda, V., & Grossiord, C. (2023). Stand structure of Central European forests matters more than climate for transpiration sensitivity to VPD. Journal of Applied Ecology, 60(5), 886–897. https://doi.org/10.1111/1365-2664.14383

Bai, Y., Liu, Y., Kueppers, L. M., Feng, X., Yu, K., Yang, X., Li, X., & Huang, J. (2021). The coupled effect of soil and atmospheric constraints on the vulnerability and water use of two desert riparian ecosystems. Agricultural and Forest Meteorology, 311, 108701. https://doi.org/10.1016/j.agrformet.2021.108701

Baldocchi, D. D., Ma, S., Rambal, S., Misson, L., Ourcival, J.-M., Limousin, J.-M., Pereira, J., & Papale, D. (2010). On the differential advantages of evergreenness and deciduousness in mediterranean oak woodlands: A flux perspective. Ecological Applications, 20(6), 1583–1597. https://doi.org/10.1890/08-2047.1

Bär, A., Nardini, A., & Mayr, S. (2018). Post-fire effects in xylem hydraulics of Picea abies, Pinus sylvestris and Fagus sylvatica. New Phytologist, 217(4), 1484–1493. https://doi.org/10.1111/nph.14916

Barbeta, A., & Peñuelas, J. (2016). Sequence of plant responses to droughts of different timescales: Lessons from holm oak (Quercus ilex) forests. Plant Ecology & Diversity, 9(4), 321–338. https://doi.org/10.1080/17550874.2016.1212288

Beck, H. E., Zimmermann, N. E., McVicar, T. R., Vergopolan, N., Berg, A., & Wood, E. F. (2018). Present and future Köppen-Geiger climate classification maps at 1-km resolution. Scientific Data, 5(1), 180214. https://doi.org/10.1038/sdata.2018.214

Bittencourt, P., Rowland, L., Sitch, S., Poyatos, R., Miralles, D. G., & Mencuccini, M. (2023). Bridging Scales: An Approach to Evaluate the Temporal Patterns of Global Transpiration Products Using Tree-Scale Sap Flow Data. Journal of Geophysical Research: Biogeosciences, 128(3), e2022JG007308. https://doi.org/10.1029/2022JG007308

Blume, T., Schneider, L., & Güntner, A. (2022). Comparative analysis of throughfall observations in six different forest stands: Influence of seasons, rainfall- and stand characteristics. Hydrological Processes, 36(3), e14461. https://doi.org/10.1002/hyp.14461

Bollmeyer, C., Keller, J. D., Ohlwein, C., Wahl, S., Crewell, S., Friederichs, P., Hense, A., Keune, J., Kneifel, S., Pscheidt, I., Redl, S., & Steinke, S. (2015). Towards a high-resolution regional reanalysis for the European CORDEX domain. Quarterly Journal of the Royal Meteorological Society, 141(686), 1–15. https://doi.org/10.1002/qj.2486

Bonan, G. B., Levis, S., Kergoat, L., & Oleson, K. W. (2002). Landscapes as patches of plant functional types: An integrating concept for climate and ecosystem models. Global Biogeochemical Cycles, 16(2), 5–1. https://doi.org/10.1029/2000GB001360

Bonan, G. B., Williams, M., Fisher, R. A., & Oleson, K. W. (2014). Modeling stomatal conductance in the earth system: Linking leaf water-use efficiency and water transport along the soil–plant–atmosphere continuum. Geoscientific Model Development, 7(5), 2193–2222. https://doi.org/10.5194/gmd-7-2193-2014

Buras, A., & Menzel, A. (2019a). Projecting Tree Species Composition Changes of European Forests for 2061–2090 Under RCP 4.5 and RCP 8.5 Scenarios. Frontiers in Plant Science, 9. https://www.frontiersin.org/articles/10.3389/fpls.2018.01986

Buras, A., & Menzel, A. (2019b). Projecting Tree Species Composition Changes of European Forests for 2061–2090 Under RCP 4.5 and RCP 8.5 Scenarios. Frontiers in Plant Science, 9. https://www.frontiersin.org/articles/10.3389/fpls.2018.01986

Burlett, R., Parise, C., Capdeville, G., Cochard, H., Lamarque, L. J., King, A., & Delzon, S. (2022). Measuring xylem hydraulic vulnerability for long-vessel species: An improved methodology with the flow centrifugation technique. Annals of Forest Science, 79(1), 5. https://doi.org/10.1186/s13595-022-01124-0

Butler, E. E., Wythers, K. R., Flores-Moreno, H., Ricciuto, D. M., Datta, A., Banerjee, A., Atkin, O. K., Kattge, J., Thornton, P. E., Anand, M., Burrascano, S., Byun, C., Cornelissen, J. H. C., Forey, E., Jansen, S., Kramer, K., Minden, V., & Reich, P. B. (2022). Increasing Functional Diversity in a Global Land Surface Model Illustrates Uncertainties Related to Parameter Simplification. Journal of Geophysical Research: Biogeosciences, 127(3), e2021JG006606. https://doi.org/10.1029/2021JG006606

Caquet, B., Barigah, T. S., Cochard, H., Montpied, P., Collet, C., Dreyer, E., & Epron, D. (2009). Hydraulic properties of naturally regenerated beech saplings respond to canopy opening. Tree Physiology, 29(11), 1395–1405. https://doi.org/10.1093/treephys/tpp067

Carevic, F., Fernández, M., Alejano, R., & Vázquez-Piqué, J. (2014). Xylem cavitation affects the recovery of plant water status and consequently acorn production in a holm oak open woodland. Acta Physiologiae Plantarum, 36(12), 3283–3290. https://doi.org/10.1007/s11738-014-1694-6

Charra-Vaskou, K., Charrier, G., Wortemann, R., Beikircher, B., Cochard, H., Ameglio, T., & Mayr, S. (2012). Drought and frost resistance of trees: A comparison of four species at different sites and altitudes. Annals of Forest Science, 69(3), 325–333. https://doi.org/10.1007/s13595-011-0160-5

Choat, B., Brodribb, T. J., Brodersen, C. R., Duursma, R. A., López, R., & Medlyn, B. E. (2018). Triggers of tree mortality under drought. Nature, 558(7711), Article 7711. https://doi.org/10.1038/s41586-018-0240-x

Choat, B., Jansen, S., Brodribb, T. J., Cochard, H., Delzon, S., Bhaskar, R., Bucci, S. J., Feild, T. S., Gleason, S. M., Hacke, U. G., Jacobsen, A. L., Lens, F., Maherali, H., Martínez-Vilalta, J., Mayr, S., Mencuccini, M., Mitchell, P. J., Nardini, A., Pittermann, J., … Zanne, A. E. (2012). Global convergence in the vulnerability of forests to drought. Nature, 491(7426), 752–755. https://doi.org/10.1038/nature11688

Christoffersen, B. O., Gloor, M., Fauset, S., Fyllas, N. M., Galbraith, D. R., Baker, T. R., Kruijt, B., Rowland, L., Fisher, R. A., Binks, O. J., Sevanto, S., Xu, C., Jansen, S., Choat, B., Mencuccini, M., McDowell, N. G., & Meir, P. (2016). Linking hydraulic traits to tropical forest function in a size-structured and trait-driven model (TFS v.1-Hydro). Geosci. Model Dev., 9(11), 4227–4255. https://doi.org/10.5194/gmd-9-4227-2016

Cochard, H., Badel, E., Herbette, S., Delzon, S., Choat, B., & Jansen, S. (2013). Methods for measuring plant vulnerability to cavitation: A critical review. Journal of Experimental Botany, 64(15), 4779–4791. https://doi.org/10.1093/jxb/ert193

Colin Prentice, I., Sykes, M. T., & Cramer, W. (1993). A simulation model for the transient effects of climate change on forest landscapes. Ecological Modelling, 65(1), 51–70. https://doi.org/10.1016/0304-3800(93)90126-D

COSMO-REA6. (2019). COSMO Regional Reanalysis (COSMO-REA6) [Dataset]. https://reanalysis.meteo.uni-bonn.de/?COSMO-REA6

CTSM. (2022). Community Terrestrial Systems Model (includes the Community Land Model of CESM) [CTSM] [Software] [Fortran]. Earth System Community Modeling Portal. https://github.com/ESCOMP/CTSM (Original work published 2017)

David, T. S., Henriques, M. O., Kurz-Besson, C., Nunes, J., Valente, F., Vaz, M., Pereira, J. S., Siegwolf, R., Chaves, M. M., Gazarini, L. C., & David, J. S. (2007). Water-use strategies in two co-occurring Mediterranean evergreen oaks: Surviving the summer drought. Tree Physiology, 27(6), 793–803. https://doi.org/10.1093/treephys/27.6.793

De Kauwe, M. G., Kala, J., Lin, Y.-S., Pitman, A. J., Medlyn, B. E., Duursma, R. A., Abramowitz, G., Wang, Y.-P., & Miralles, D. G. (2015). A test of an optimal stomatal conductance scheme within the CABLE land surface model. Geoscientific Model Development, 8(2), 431–452. https://doi.org/10.5194/gmd-8-431-2015

De Kauwe, M. G., Sabot, M. E. B., Medlyn, B. E., Pitman, A. J., Meir, P., Cernusak, L. A., Gallagher, R. V., Ukkola, A. M., Rifai, S. W., & Choat, B. (2022). Towards species-level forecasts of drought-induced tree mortality risk. New Phytologist, 235(1), 94–110. https://doi.org/10.1111/nph.18129

de Rigo, D., & Caudullo, G. (2016). Quercus ilex in Europe: Distribution, habitat, usage and threats. In European Atlas of Forest Tree Species. Publication Office of the European Union. https://forest.jrc.ec.europa.eu/en/european-atlas/atlas-download-page/

Deng, L., Peng, C., Kim, D.-G., Li, J., Liu, Y., Hai, X., Liu, Q., Huang, C., Shangguan, Z., & Kuzyakov, Y. (2021). Drought effects on soil carbon and nitrogen dynamics in global natural ecosystems. Earth-Science Reviews, 214, 103501. https://doi.org/10.1016/j.earscirev.2020.103501

Domec, J.-C., & Gartner, B. L. (2001). Cavitation and water storage capacity in bole xylem segments of mature and young Douglas-fir trees. Trees, 15(4), 204–214. https://doi.org/10.1007/s004680100095

Domec, J.-C., Lachenbruch, B., Pruyn, M. L., & Spicer, R. (2012). Effects of age-related increases in sapwood area, leaf area, and xylem conductivity on height-related hydraulic costs in two contrasting coniferous species. Annals of Forest Science, 69(1), 17–27. https://doi.org/10.1007/s13595-011-0154-3

Domec Jean-Christophe, Lachenbruch Barbara, Meinzer Frederick C., Woodruff David R., Warren Jeffrey M., & McCulloh Katherine A. (2008). Maximum height in a conifer is associated with conflicting requirements for xylem design. Proceedings of the National Academy of Sciences, 105(33), 12069–12074. https://doi.org/10.1073/pnas.0710418105

Duveiller, G., Fasbender, D., & Meroni, M. (2016). Revisiting the concept of a symmetric index of agreement for continuous datasets. Scientific Reports, 6(1), Article 1. https://doi.org/10.1038/srep19401

Eamus, D., Huete, A., & Yu, Q. (2016). Vegetation dynamics. A synthesis of plant ecophysiology, remote sensing and modelling. Cambridge University Press.

Eller, C. B., Rowland, L., Mencuccini, M., Rosas, T., Williams, K., Harper, A., Medlyn, B. E., Wagner, Y., Klein, T., Teodoro, G. S., Oliveira, R. S., Matos, I. S., Rosado, B. H. P., Fuchs, K., Wohlfahrt, G., Montagnani, L., Meir, P., Sitch, S., & Cox, P. M. (2020). Stomatal optimization based on xylem hydraulics (SOX) improves land surface model simulation of vegetation responses to climate. New Phytologist, 226(6), 1622–1637. https://doi.org/10.1111/nph.16419

Fatichi, S., Pappas, C., & Ivanov, V. Y. (2016). Modeling plant–water interactions: An ecohydrological overview from the cell to the global scale. WIREs Water, 3(3), 327–368. https://doi.org/10.1002/wat2.1125

Fichtler, E., & Worbes, M. (2012). Wood anatomical variables in tropical trees and their relation to site conditions and individual tree morphology. IAWA Journal, 33(2), 119–140. https://doi.org/10.1163/22941932-90000084

Flo, V., Martínez-Vilalta, J., Mencuccini, M., Granda, V., Anderegg, W. R. L., & Poyatos, R. (2021). Climate and functional traits jointly mediate tree water-use strategies. New Phytologist, 231(2), 617–630. https://doi.org/10.1111/nph.17404

Forner, A., Valladares, F., & Aranda, I. (2018). Mediterranean trees coping with severe drought: Avoidance might not be safe. Environmental and Experimental Botany, 155, 529–540. https://doi.org/10.1016/j.envexpbot.2018.08.006

Franklin, O., Harrison, S. P., Dewar, R., Farrior, C. E., Brännström, Å., Dieckmann, U., Pietsch, S., Falster, D., Cramer, W., Loreau, M., Wang, H., Mäkelä, A., Rebel, K. T., Meron, E., Schymanski, S. J., Rovenskaya, E., Stocker, B. D., Zaehle, S., Manzoni, S., … Prentice, I. C. (2020). Organizing principles for vegetation dynamics. Nature Plants, 6(5), Article 5. https://doi.org/10.1038/s41477-020-0655-x

Franks, P. J. (2004). Stomatal control and hydraulic conductance, with special reference to tall trees. Tree Physiology, 24(8), 865–878. https://doi.org/10.1093/treephys/24.8.865

Fu, Z., Ciais, P., Prentice, I. C., Gentine, P., Makowski, D., Bastos, A., Luo, X., Green, J. K., Stoy, P. C., Yang, H., & Hajima, T. (2022). Atmospheric dryness reduces photosynthesis along a large range of soil water deficits. Nature Communications, 13(1), Article 1. https://doi.org/10.1038/s41467-022-28652-7

Fuchs, S., Leuschner, C., Mathias Link, R., & Schuldt, B. (2021). Hydraulic variability of three temperate broadleaf tree species along a water availability gradient in central Europe. New Phytologist, 231(4), 1387–1400. https://doi.org/10.1111/nph.17448

Fyllas, N. M., Michelaki, C., Galanidis, A., Evangelou, E., Zaragoza-Castells, J., Dimitrakopoulos, P. G., Tsadilas, C., Arianoutsou, M., & Lloyd, J. (2020). Functional Trait Variation Among and Within Species and Plant Functional Types in Mountainous Mediterranean Forests. Frontiers in Plant Science, 11. https://www.frontiersin.org/articles/10.3389/fpls.2020.00212

Gleason, S. M., Westoby, M., Jansen, S., Choat, B., Hacke, U. G., Pratt, R. B., Bhaskar, R., Brodribb, T. J., Bucci, S. J., Cao, K.-F., Cochard, H., Delzon, S., Domec, J.-C., Fan, Z.-X., Feild, T. S., Jacobsen, A. L., Johnson, D. M., Lens, F., Maherali, H., … Zanne, A. E. (2016). Weak tradeoff between xylem safety and xylem-specific hydraulic efficiency across the world's woody plant species. New Phytologist, 209(1), 123–136. https://doi.org/10.1111/nph.13646

Gortan, E., Nardini, A., Gascó, A., & Salleo, S. (2009). The hydraulic conductance of Fraxinus ornus leaves is constrained by soil water availability and coordinated with gas exchange rates. Tree Physiology, 29(4), 529–539. https://doi.org/10.1093/treephys/tpn053

Granier, A., Bréda, N., Longdoz, B., Gross, P., & Ngao, J. (2008). Ten years of fluxes and stand growth in a young beech forest at Hesse, North-eastern France. Annals of Forest Science, 65(7), 704–704. https://doi.org/10.1051/forest:2008052

Granier, A., Ceschia, E., Damesin, C., Dufrêne, E., Epron, D., Gross, P., Lebaube, S., Le Dantec, V., Le Goff, N., Lemoine, D., Lucot, E., Ottorini, J. M., Pontailler, J. Y., & Saugier, B. (2000). The carbon balance of a young Beech forest. Functional Ecology, 14(3), 312–325. https://doi.org/10.1046/j.1365-2435.2000.00434.x

Haberstroh, S., & Werner, C. (2022). The role of species interactions for forest resilience to drought. Plant Biology, n/a(n/a). https://doi.org/10.1111/plb.13415

Hacke, U. G., Sperry, J. S., Wheeler, J. K., & Castro, L. (2006). Scaling of angiosperm xylem structure with safety and efficiency. Tree Physiology, 26(6), 689–701. https://doi.org/10.1093/treephys/26.6.689

Hacke, U., & Sauter, J. J. (1995). Vulnerability of xylem to embolism in relation to leaf water potential and stomatal conductance in Fagus sylvatica f. Purpurea and Populus balsamifera. Journal of Experimental Botany, 46(9), 1177–1183. https://doi.org/10.1093/jxb/46.9.1177

Hajek, P., Kurjak, D., von Wühlisch, G., Delzon, S., & Schuldt, B. (2016). Intraspecific Variation in Wood Anatomical, Hydraulic, and Foliar Traits in Ten European Beech Provenances Differing in Growth Yield. Frontiers in Plant Science, 7. https://www.frontiersin.org/articles/10.3389/fpls.2016.00791

Hammond, W. M., Williams, A. P., Abatzoglou, J. T., Adams, H. D., Klein, T., López, R., Sáenz-Romero, C., Hartmann, H., Breshears, D. D., & Allen, C. D. (2022). Global field observations of tree die-off reveal hotter-drought fingerprint for Earth's forests. Nature Communications, 13(1), Article 1. https://doi.org/10.1038/s41467-022-29289-2

He, X., Pan, M., Wei, Z., Wood, E. F., & Sheffield, J. (2020). A Global Drought and Flood Catalogue from 1950 to 2016. Bulletin of the American Meteorological Society, 101(5), E508–E535. https://doi.org/10.1175/BAMS-D-18-0269.1

Heinrich, I., Balanzategui, D., Bens, O., Blasch, G., Blume, T., Böttcher, F., Borg, E., Brademann, B., Brauer, A., Conrad, C., Dietze, E., Dräger, N., Fiener, P., Gerke, H. H., Güntner, A., Heine, I., Helle, G., Herbrich, M., Harfenmeister, K., … Wilken, F. (2018). Interdisciplinary Geo-ecological Research across Time Scales in the Northeast German Lowland Observatory (TERENO-NE). Vadose Zone Journal, 17(1), 180116. https://doi.org/10.2136/vzj2018.06.0116

Hochberg, U., Rockwell, F. E., Holbrook, N. M., & Cochard, H. (2018). Iso/Anisohydry: A Plant–Environment Interaction Rather Than a Simple Hydraulic Trait. Trends in Plant Science, 23(2), 112–120. https://doi.org/10.1016/j.tplants.2017.11.002

Houston Durrant, T., de Rigo, D., & Caudullo, G. (2016). Fagus sylvatica and other beeches in Europe: Distribution, habitat, usage and threats. In European Atlas of Forest Tree Species. Publication Office of the European Union. https://forest.jrc.ec.europa.eu/en/european-atlas/atlas-download-page/

Huber, A. E., Melcher, P. J., Piñeros, M. A., Setter, T. L., & Bauerle, T. L. (2019). Signal coordination before, during and after stomatal closure in response to drought stress. New Phytologist, 224(2), 675–688. https://doi.org/10.1111/nph.16082

Jiménez-Rodríguez, C. D. (2023). The role of the intraspecific variability of hydraulic traits for modelling the plant water use in different European forest ecosystems: Scripts, model output, and parameter files [Dataset]. https://doi.org/10.5281/zenodo.8019682

Jiménez-Rodríguez, C. D., Sulis, M., & Schymanski, S. (2022). Exploring the role of bedrock representation on plant transpiration response during dry periods at four forested sites in Europe. Biogeosciences, 19(14), 3395–3423. https://doi.org/10.5194/bg-19-3395-2022

Joetzjer, E., Maignan, F., Chave, J., Goll, D., Poulter, B., Barichivich, J., Maréchaux, I., Luyssaert, S., Guimberteau, M., Naudts, K., Bonal, D., & Ciais, P. (2022). Effect of tree demography and flexible root water uptake for modeling the carbon and water cycles of Amazonia. Ecological Modelling, 469, 109969. https://doi.org/10.1016/j.ecolmodel.2022.109969

Johnson, D. M., McCulloh, K. A., Woodruff, D. R., & Meinzer, F. C. (2012). Hydraulic safety margins and embolism reversal in stems and leaves: Why are conifers and angiosperms so different? Plant Science, 195, 48–53. https://doi.org/10.1016/j.plantsci.2012.06.010

Joshi, J., Stocker, B. D., Hofhansl, F., Zhou, S., Dieckmann, U., & Prentice, I. C. (2022). Towards a unified theory of plant photosynthesis and hydraulics. Nature Plants, 8(11), Article 11. https://doi.org/10.1038/s41477-022-01244-5

Kennedy, D., Swenson, S., Oleson, K. W., Lawrence, D. M., Fisher, R., Lola da Costa, A. C., & Gentine, P. (2019). Implementing Plant Hydraulics in the Community Land Model, Version 5. Journal of Advances in Modeling Earth Systems, 11(2), 485–513. https://doi.org/10.1029/2018MS001500

Kirchen, G., Calvaruso, C., Granier, A., Redon, P.-O., Van der Heijden, G., Bréda, N., & Turpault, M.-P. (2017). Local soil type variability controls the water budget and stand productivity in a beech forest. Forest Ecology and Management, 390, 89–103. https://doi.org/10.1016/j.foreco.2016.12.024

Klein, T., Zeppel, M. J. B., Anderegg, W. R. L., Bloemen, J., De Kauwe, M. G., Hudson, P., Ruehr, N. K., Powell, T. L., von Arx, G., & Nardini, A. (2018). Xylem embolism refilling and resilience against drought-induced mortality in woody plants: Processes and trade-offs. Ecological Research, 33(5), 839–855. https://doi.org/10.1007/s11284-018-1588-y

Knüver, T., Bär, A., Ganthaler, A., Gebhardt, T., Grams, T. E. E., Häberle, K.-H., Hesse, B. D., Losso, A., Tomedi, I., Mayr, S., & Beikircher, B. (2022). Recovery after long-term summer drought: Hydraulic measurements reveal legacy effects in trunks of Picea abies but not in Fagus sylvatica. Plant Biology, n/a(n/a). https://doi.org/10.1111/plb.13444

Konings, A. G., & Gentine, P. (2017). Global variations in ecosystem-scale isohydricity. Global Change Biology, 23(2), 891–905. https://doi.org/10.1111/gcb.13389

Lansu, E. M., van Heerwaarden, C. C., Stegehuis, A. I., & Teuling, A. J. (2020). Atmospheric Aridity and Apparent Soil Moisture Drought in European Forest During Heat Waves. Geophysical Research Letters, 47(6), e2020GL087091. https://doi.org/10.1029/2020GL087091

Lavoir, A.-V., Staudt, M., Schnitzler, J. P., Landais, D., Massol, F., Rocheteau, A., Rodriguez, R., Zimmer, I., & Rambal, S. (2009). Drought reduced monoterpene emissions from the

evergreen Mediterranean oak Quercus ilex: Results from a throughfall displacement experiment. Biogeosciences, 6(7), 1167–1180. https://doi.org/10.5194/bg-6-1167-2009

Lawrence, D. M., Fisher, R. A., Koven, C. D., Oleson, K. W., Swenson, S. C., Bonan, G., Collier, N., Ghimire, B., van Kampenhout, L., Kennedy, D., Kluzek, E., Lawrence, P. J., Li, F., Li, H., Lombardozzi, D., Riley, W. J., Sacks, W. J., Shi, M., Vertenstein, M., … Zeng, X. (2019). The Community Land Model Version 5: Description of New Features, Benchmarking, and Impact of Forcing Uncertainty. Journal of Advances in Modeling Earth Systems, 11(12), 4245–4287. https://doi.org/10.1029/2018MS001583

Lawrence, P. J., & Chase, T. N. (2007). Representing a new MODIS consistent land surface in the Community Land Model (CLM 3.0). Journal of Geophysical Research: Biogeosciences, 112(G1). https://doi.org/10.1029/2006JG000168

Lawrence, P. J., & Chase, T. N. (2010). Investigating the climate impacts of global land cover change in the community climate system model. International Journal of Climatology, 30(13), 2066–2087. https://doi.org/10.1002/joc.2061

Lemoine, D., Cochard, H., & Granier, A. (2002). Within crown variation in hydraulic architecture in beech (Fagus sylvatica L): Evidence for a stomatal control of xylem embolism. Annals of Forest Science, 59(1), 19–27. https://doi.org/10.1051/forest:2001002

Lemoine, D., Jacquemin, S., & Granier, A. (2002). Beech (Fagus sylvatica L.) branches show acclimation of xylem anatomy and hydraulic properties to increased light after thinning. Annals of Forest Science, 59(7), 761–766. https://doi.org/10.1051/forest:2002062

Leuschner, C. (2020). Drought response of European beech (Fagus sylvatica L.)—A review. Perspectives in Plant Ecology, Evolution and Systematics, 47, 125576. https://doi.org/10.1016/j.ppees.2020.125576

Leuschner, C., & Meier, I. C. (2018). The ecology of Central European tree species: Trait spectra, functional trade-offs, and ecological classification of adult trees. Perspectives in Plant Ecology, Evolution and Systematics, 33, 89–103. https://doi.org/10.1016/j.ppees.2018.05.003

Li, L., Yang, Z.-L., Matheny, A. M., Zheng, H., Swenson, S. C., Lawrence, D. M., Barlage, M., Yan, B., McDowell, N. G., & Leung, L. R. (2021). Representation of Plant Hydraulics in the Noah-MP Land Surface Model: Model Development and Multiscale Evaluation. Journal of Advances in Modeling Earth Systems, 13(4), e2020MS002214. https://doi.org/10.1029/2020MS002214

Liang, S., Zhang, X., Xiao, Z., Cheng, J., Liu, Q., & Zhao, X. (2014). Leaf Area Index. In S. Liang, X. Zhang, Z. Xiao, J. Cheng, Q. Liu, & X. Zhao (Eds.), Global LAnd Surface Satellite (GLASS) Products: Algorithms, Validation and Analysis (pp. 3–31). Springer International Publishing. https://doi.org/10.1007/978-3-319-02588-9_2

Liang, S., Zhao, X., Liu, S., Yuan, W., Cheng, X., Xiao, Z., Zhang, X., Liu, Q., Cheng, J., Tang, H., Qu, Y., Bo, Y., Qu, Y., Ren, H., Yu, K., & Townshend, J. (2013). A long-term Global LAnd Surface Satellite (GLASS) data-set for environmental studies. International Journal of Digital Earth, 6(sup1), 5–33. https://doi.org/10.1080/17538947.2013.805262

Limousin, J.-M., Longepierre, D., Huc, R., & Rambal, S. (2010). Change in hydraulic traits of Mediterranean Quercus ilex subjected to long-term throughfall exclusion. Tree Physiology, 30(8), 1026–1036. https://doi.org/10.1093/treephys/tpq062

Lin, Y.-S., Medlyn, B. E., Duursma, R. A., Prentice, I. C., Wang, H., Baig, S., Eamus, D., de Dios, V. R., Mitchell, P., Ellsworth, D. S., de Beeck, M. O., Wallin, G., Uddling, J., Tarvainen, L., Linderson, M.-L., Cernusak, L. A., Nippert, J. B., Ocheltree, T. W., Tissue, D. T., … Wingate, L. (2015). Optimal stomatal behaviour around the world. Nature Climate Change, 5(5), Article 5. https://doi.org/10.1038/nclimate2550

Lindroth, A., Holst, J., Linderson, M.-L., Aurela, M., Biermann, T., Heliasz, M., Chi, J., Ibrom, A., Kolari, P., Klemedtsson, L., Krasnova, A., Laurila, T., Lehner, I., Lohila, A., Mammarella, I., Mölder, M., Löfvenius, M. O., Peichl, M., Pilegaard, K., … Nilsson, M. (2020). Effects of drought and meteorological forcing on carbon and water fluxes in Nordic forests during the dry summer of 2018. Philosophical Transactions of the Royal Society B: Biological Sciences, 375(1810), 20190516. https://doi.org/10.1098/rstb.2019.0516

Liu, Y., Holtzman, N. M., & Konings, A. G. (2021). Global ecosystem-scale plant hydraulic traits retrieved using model–data fusion. Hydrology and Earth System Sciences, 25(5), 2399–2417. https://doi.org/10.5194/hess-25-2399-2021

Liu, Y., Kumar, M., Katul, G. G., Feng, X., & Konings, A. G. (2020). Plant hydraulics accentuates the effect of atmospheric moisture stress on transpiration. Nature Climate Change, 10(7), Article 7. https://doi.org/10.1038/s41558-020-0781-5

Lobo, A., Torres-Ruiz, J. M., Burlett, R., Lemaire, C., Parise, C., Francioni, C., Truffaut, L., Tomášková, I., Hansen, J. K., Kjær, E. D., Kremer, A., & Delzon, S. (2018). Assessing inter- and intraspecific variability of xylem vulnerability to embolism in oaks. Forest Ecology and Management, 424, 53–61. https://doi.org/10.1016/j.foreco.2018.04.031

Lorenzo-Lacruz, J., Vicente-Serrano, S. M., López-Moreno, J. I., Beguería, S., García-Ruiz, J. M., & Cuadrat, J. M. (2010). The impact of droughts and water management on various hydrological systems in the headwaters of the Tagus River (central Spain). Journal of Hydrology, 386(1), 13–26. https://doi.org/10.1016/j.jhydrol.2010.01.001

Lu, Y., Sloan, B., Thompson, S. E., Konings, A. G., Bohrer, G., Matheny, A., & Feng, X. (2022). Intra-Specific Variability in Plant Hydraulic Parameters Inferred From Model Inversion of Sap Flux Data. Journal of Geophysical Research: Biogeosciences, 127(6), e2021JG006777. https://doi.org/10.1029/2021JG006777

Lübbe, T., Lamarque, L. J., Delzon, S., Torres Ruiz, J. M., Burlett, R., Leuschner, C., & Schuldt, B. (2022). High variation in hydraulic efficiency but not xylem safety between roots and branches in four temperate broad-leaved tree species. Functional Ecology, 36(3), 699–712. https://doi.org/10.1111/1365-2435.13975

Mackay, D. S., Roberts, D. E., Ewers, B. E., Sperry, J. S., McDowell, N. G., & Pockman, W. T. (2015). Interdependence of chronic hydraulic dysfunction and canopy processes can improve integrated models of tree response to drought. Water Resources Research, 51(8), 6156–6176. https://doi.org/10.1002/2015WR017244

Martínez-Vilalta, J., Prat, E., Oliveras, I., & Piñol, J. (2002). Xylem hydraulic properties of roots and stems of nine Mediterranean woody species. Oecologia, 133(1), 19–29. https://doi.org/10.1007/s00442-002-1009-2

Martin-StPaul, N. K., Longepierre, D., Huc, R., Delzon, S., Burlett, R., Joffre, R., Rambal, S., & Cochard, H. (2014). How reliable are methods to assess xylem vulnerability to cavitation? The issue of 'open vessel' artifact in oaks. Tree Physiology, 34(8), 894–905. https://doi.org/10.1093/treephys/tpu059

Matheny, A. M. (2021). Stressors Reveal Ecosystems' Hidden Characteristics. Journal of Geophysical Research: Biogeosciences, 126(8), e2021JG006462. https://doi.org/10.1029/2021JG006462

Matheny, A. M., Mirfenderesgi, G., & Bohrer, G. (2017). Trait-based representation of hydrological functional properties of plants in weather and ecosystem models. Plant Diversity, 39(1), 1–12. https://doi.org/10.1016/j.pld.2016.10.001

Mauri, A., Girardello, M., Strona, G., Beck, P. S. A., Forzieri, G., Caudullo, G., Manca, F., & Cescatti, A. (2022). EU-Trees4F, a dataset on the future distribution of European tree species. Scientific Data, 9(1), Article 1. https://doi.org/10.1038/s41597-022-01128-5

McDowell, N. G., Sapes, G., Pivovaroff, A., Adams, H. D., Allen, C. D., Anderegg, W. R. L., Arend, M., Breshears, D. D., Brodribb, T., Choat, B., Cochard, H., De Cáceres, M., De Kauwe, M. G., Grossiord, C., Hammond, W. M., Hartmann, H., Hoch, G., Kahmen, A., Klein, T., … Xu, C. (2022). Mechanisms of woody-plant mortality under rising drought, CO2 and vapour pressure deficit. Nature Reviews Earth & Environment, 3(5), Article 5. https://doi.org/10.1038/s43017-022-00272-1

Medlyn, B. E., Duursma, R. A., Eamus, D., Ellsworth, D. S., Prentice, I. C., Barton, C. V. M., Crous, K. Y., De Angelis, P., Freeman, M., & Wingate, L. (2011). Reconciling the optimal and empirical approaches to modelling stomatal conductance. Global Change Biology, 17(6), 2134–2144. https://doi.org/10.1111/j.1365-2486.2010.02375.x

Meinzer, F. C., Johnson, D. M., Lachenbruch, B., McCulloh, K. A., & Woodruff, D. R. (2009). Xylem hydraulic safety margins in woody plants: Coordination of stomatal control of xylem tension with hydraulic capacitance. Functional Ecology, 23(5), 922–930. https://doi.org/10.1111/j.1365-2435.2009.01577.x

Meinzer, F. C., & McCulloh, K. A. (2013). Xylem recovery from drought-induced embolism: Where is the hydraulic point of no return? Tree Physiology, 33(4), 331–334. https://doi.org/10.1093/treephys/tpt022

Mencuccini, M., Manzoni, S., & Christoffersen, B. (2019). Modelling water fluxes in plants: From tissues to biosphere. New Phytologist, 222(3), 1207–1222. https://doi.org/10.1111/nph.15681

Mirfenderesgi, G., Matheny, A. M., & Bohrer, G. (2019). Hydrodynamic trait coordination and cost–benefit trade-offs throughout the isohydric–anisohydric continuum in trees. Ecohydrology, 12(1), e2041. https://doi.org/10.1002/eco.2041

Moreno, A., Neumann, M., & Hasenauer, H. (2017). Forest structures across Europe. Geoscience Data Journal, 4(1), 17–28. https://doi.org/10.1002/gdj3.45

Mrad, A., Domec, J.-C., Huang, C.-W., Lens, F., & Katul, G. (2018). A network model links wood anatomy to xylem tissue hydraulic behaviour and vulnerability to cavitation. Plant, Cell & Environment, 41(12), 2718–2730. https://doi.org/10.1111/pce.13415

Mrad, A., Sevanto, S., Domec, J.-C., Liu, Y., Nakad, M., & Katul, G. (2019). A Dynamic Optimality Principle for Water Use Strategies Explains Isohydric to Anisohydric Plant Responses to Drought. Frontiers in Forests and Global Change, 2. https://www.frontiersin.org/articles/10.3389/ffgc.2019.00049

Nelson, J. A., Pérez-Priego, O., Zhou, S., Poyatos, R., Zhang, Y., Blanken, P. D., Gimeno, T. E., Wohlfahrt, G., Desai, A. R., Gioli, B., Limousin, J.-M., Bonal, D., Paul-Limoges, E., Scott, R. L., Varlagin, A., Fuchs, K., Montagnani, L., Wolf, S., Delpierre, N., … Jung, M. (2020). Ecosystem transpiration and evaporation: Insights from three water flux partitioning methods across FLUXNET sites. Global Change Biology, 26(12), 6916–6930. https://doi.org/10.1111/gcb.15314

Novick, K. A., Ficklin, D. L., Baldocchi, D., Davis, K. J., Ghezzehei, T. A., Konings, A. G., MacBean, N., Raoult, N., Scott, R. L., Shi, Y., Sulman, B. N., & Wood, J. D. (2022). Confronting the water potential information gap. Nature Geoscience, 15(3), Article 3. https://doi.org/10.1038/s41561-022-00909-2

Novick, K. A., Konings, A. G., & Gentine, P. (2019). Beyond soil water potential: An expanded view on isohydricity including land–atmosphere interactions and phenology. Plant, Cell & Environment, 42(6), 1802–1815. https://doi.org/10.1111/pce.13517

Oddi, L., Migliavacca, M., Cremonese, E., Filippa, G., Vacchiano, G., Siniscalco, C., Cella, U. M. di, & Galvagno, M. (2022). Contrasting responses of forest growth and carbon sequestration to heat and drought in the Alps. Environmental Research Letters, 17(4), 045015. https://doi.org/10.1088/1748-9326/ac5b3a

Pappas, C., Fatichi, S., & Burlando, P. (2016). Modeling terrestrial carbon and water dynamics across climatic gradients: Does plant trait diversity matter? New Phytologist, 209(1), 137–151. https://doi.org/10.1111/nph.13590

Peguero-Pina, J. J., Sancho-Knapik, D., Barrón, E., Camarero, J. J., Vilagrosa, A., & Gil-Pelegrín, E. (2014). Morphological and physiological divergences within Quercus ilex support the existence of different ecotypes depending on climatic dryness. Annals of Botany, 114(2), 301–313.

Peiffer, M., Bréda, N., Badeau, V., & Granier, A. (2014). Disturbances in European beech water relation during an extreme drought. Annals of Forest Science, 71(7), Article 7. https://doi.org/10.1007/s13595-014-0383-3

Pelletier, J. D., Broxton, P. D., Hazenberg, P., Zeng, X., Troch, P. A., Niu, G.-Y., Williams, Z., Brunke, M. A., & Gochis, D. (2016). A gridded global data set of soil, intact regolith, and sedimentary deposit thicknesses for regional and global land surface modeling. Journal of

Advances in Modeling Earth Systems, 8(1), 41–65. https://doi.org/10.1002/2015MS000526

Peñuelas, J., & Filella, I. (2003). Deuterium labelling of roots provides evidence of deep water access and hydraulic lift by Pinus nigra in a Mediterranean forest of NE Spain. Environmental and Experimental Botany, 49(3), 201–208. https://doi.org/10.1016/S0098-8472(02)00070-9

Pereira, L., Domingues-Junior, A. P., Jansen, S., Choat, B., & Mazzafera, P. (2018). Is embolism resistance in plant xylem associated with quantity and characteristics of lignin? Trees, 32(2), 349–358. https://doi.org/10.1007/s00468-017-1574-y

Powers, J. S., Vargas G., G., Brodribb, T. J., Schwartz, N. B., Pérez-Aviles, D., Smith-Martin, C. M., Becknell, J. M., Aureli, F., Blanco, R., Calderón-Morales, E., Calvo-Alvarado, J. C., Calvo-Obando, A. J., Chavarría, M. M., Carvajal-Vanegas, D., Jiménez-Rodríguez, C. D., Murillo Chacon, E., Schaffner, C. M., Werden, L. K., Xu, X., & Medvigy, D. (2020). A catastrophic tropical drought kills hydraulically vulnerable tree species. Global Change Biology, 26(5), 3122–3133. https://doi.org/10.1111/gcb.15037

Poyatos, R., Granda, V., Flo, V., Adams, M. A., Adorján, B., Aguadé, D., Aidar, M. P. M., Allen, S., Alvarado-Barrientos, M. S., Anderson-Teixeira, K. J., Aparecido, L. M., Arain, M. A., Aranda, I., Asbjornsen, H., Baxter, R., Beamesderfer, E., Berry, Z. C., Berveiller, D., Blakely, B., … Martínez-Vilalta, J. (2021). Global transpiration data from sap flow measurements: The SAPFLUXNET database. Earth System Science Data, 13(6), 2607–2649. https://doi.org/10.5194/essd-13-2607-2021

Poyatos, R., Granda, V., Flo, V., Molowny-Horas, R., Steppe, K., Mencuccini, M., & Martínez-Vilalta, J. (2020, August 4). SAPFLUXNET: A global database of sap flow measurements [Dataset]. https://doi.org/10.5281/zenodo.3971689

Preisler, Y., Hölttä, T., Grünzweig, J. M., Oz, I., Tatarinov, F., Ruehr, N. K., Rotenberg, E., & Yakir, D. (2022). The importance of tree internal water storage under drought conditions. Tree Physiology, 42(4), 771–783. https://doi.org/10.1093/treephys/tpab144

Reichstein, M., Bahn, M., Mahecha, M. D., Kattge, J., & Baldocchi, D. D. (2014). Linking plant and ecosystem functional biogeography. Proceedings of the National Academy of Sciences, 111(38), 13697–13702. https://doi.org/10.1073/pnas.1216065111

Rohatgi, A. (2022). WebPlotDigitizer—Extract data from plots, images, and maps. Webplotdigitizer: Version 4.6. https://automeris.io/WebPlotDigitizer/citation.html

Rosner, S., Heinze, B., Savi, T., & Dalla-Salda, G. (2019). Prediction of hydraulic conductivity loss from relative water loss: New insights into water storage of tree stems and branches. Physiologia Plantarum, 165(4), 843–854. https://doi.org/10.1111/ppl.12790

Sabot, M. E. B., De Kauwe, M. G., Pitman, A. J., Medlyn, B. E., Verhoef, A., Ukkola, A. M., & Abramowitz, G. (2020). Plant profit maximization improves predictions of European forest responses to drought. New Phytologist, 226(6), 1638–1655. https://doi.org/10.1111/nph.16376

Savi, T., Tintner, J., Da Sois, L., Grabner, M., Petit, G., & Rosner, S. (2019). The potential of Mid-Infrared spectroscopy for prediction of wood density and vulnerability to embolism in woody angiosperms. Tree Physiology, 39(3), 503–510. https://doi.org/10.1093/treephys/tpy112

Schirone, B., Vessella, F., & Varela, M. (2019). EUFORGEN Technical Guidelines for genetic conservation and use for Holm oak (Quercus ilex). European Forest Genetic Resources Programme (EUFORGEN). European Forest Institute. http://www.euforgen.org/fileadmin//templates/euforgen.org/upload/Publications/Technical_guidelines/Technical_guidelines_Quercus_ilex.pdf

Schoppach, R., Chun, K. P., He, Q., Fabiani, G., & Klaus, J. (2021). Species-specific control of DBH and landscape characteristics on tree-to-tree variability of sap velocity. Agricultural and Forest Meteorology, 307, 108533. https://doi.org/10.1016/j.agrformet.2021.108533

Schuldt, B., Knutzen, F., Delzon, S., Jansen, S., Müller-Haubold, H., Burlett, R., Clough, Y., & Leuschner, C. (2016). How adaptable is the hydraulic system of European beech in the face of climate change-related precipitation reduction? New Phytologist, 210(2), 443–458. https://doi.org/10.1111/nph.13798

Senf, C., Buras, A., Zang, C. S., Rammig, A., & Seidl, R. (2020). Excess forest mortality is consistently linked to drought across Europe. Nature Communications, 11(1), 6200. https://doi.org/10.1038/s41467-020-19924-1

Sergent, A. S., Varela, S. A., Barigah, T. S., Badel, E., Cochard, H., Dalla-Salda, G., Delzon, S., Fernández, M. E., Guillemot, J., Gyenge, J., Lamarque, L. J., Martinez-Meier, A., Rozenberg, P., Torres-Ruiz, J. M., & Martin-StPaul, N. K. (2020). A comparison of five methods to assess embolism resistance in trees. Forest Ecology and Management, 468, 118175. https://doi.org/10.1016/j.foreco.2020.118175

Skelton, R. P., West, A. G., & Dawson, T. E. (2015). Predicting plant vulnerability to drought in biodiverse regions using functional traits. Proceedings of the National Academy of Sciences, 112(18), 5744–5749. https://doi.org/10.1073/pnas.1503376112

Sloan, B. P., Thompson, S. E., & Feng, X. (2021). Plant hydraulic transport controls transpiration sensitivity to soil water stress. Hydrology and Earth System Sciences, 25(8), 4259–4274. https://doi.org/10.5194/hess-25-4259-2021

Song, J., Miller, G. R., Cahill, A. T., Aparecido, L. M. T., & Moore, G. W. (2020). Modeling land surface processes over a mountainous rainforest in Costa Rica using CLM4.5 and CLM5. Geoscientific Model Development, 13(11), 5147–5173. https://doi.org/10.5194/gmd-13-5147-2020

Sperry, J. S., & Love, D. M. (2015). What plant hydraulics can tell us about responses to climate-change droughts. New Phytologist, 207(1), 14–27. https://doi.org/10.1111/nph.13354

Stojnić, S., Suchocka, M., Benito-Garzón, M., Torres-Ruiz, J. M., Cochard, H., Bolte, A., Cocozza, C., Cvjetković, B., de Luis, M., Martinez-Vilalta, J., Ræbild, A., Tognetti, R., & Delzon, S. (2018). Variation in xylem vulnerability to embolism in European beech from

geographically marginal populations. Tree Physiology, 38(2), 173–185. https://doi.org/10.1093/treephys/tpx128

Sturm, J., Santos, M. J., Schmid, B., & Damm, A. (2022). Satellite data reveal differential responses of Swiss forests to unprecedented 2018 drought. Global Change Biology, 28(9), 2956–2978. https://doi.org/10.1111/gcb.16136

Terradas, J., & Savé, R. (1992). The influence of summer and winter stress and water relationships on the distribution of Quercus ilex L. Vegetatio, 99(1), 137–145. https://doi.org/10.1007/BF00118219

Tomasella, M., Nardini, A., Hesse, B. D., Machlet, A., Matyssek, R., & Häberle, K.-H. (2019). Close to the edge: Effects of repeated severe drought on stem hydraulics and non-structural carbohydrates in European beech saplings. Tree Physiology, 39(5), 717–728. https://doi.org/10.1093/treephys/tpy142

Tyree, M. T., & Cochard, H. (1996). Summer and winter embolism in oak: Impact on water relations. Annales Des Sciences Forestières, 53(2–3), 173–180. https://doi.org/10.1051/forest:19960201

UCAR. (2020). 2. CLM Technical Note—Ctsm release-clm5.0 documentation. https://escomp.github.io/ctsm-docs/versions/release-clm5.0/html/tech_note/index.html

Urli, M., Lamy, J.-B., Sin, F., Burlett, R., Delzon, S., & Porté, A. J. (2015). The high vulnerability of Quercus robur to drought at its southern margin paves the way for Quercus ilex. Plant Ecology, 216(2), 177–187. https://doi.org/10.1007/s11258-014-0426-8

Venturas, M. D., Sperry, J. S., & Hacke, U. G. (2017). Plant xylem hydraulics: What we understand, current research, and future challenges. Journal of Integrative Plant Biology, 59(6), 356–389. https://doi.org/10.1111/jipb.12534

Verheijen, L. M., Brovkin, V., Aerts, R., Bönisch, G., Cornelissen, J. H. C., Kattge, J., Reich, P. B., Wright, I. J., & van Bodegom, P. M. (2013). Impacts of trait variation through observed trait–climate relationships on performance of an Earth system model: A conceptual analysis. Biogeosciences, 10(8), 5497–5515. https://doi.org/10.5194/bg-10-5497-2013

von Wuehlisch, G. (2008). EUFORGEN Technical Guidelines for genetic conservation and use for European beech (Fagus sylvatica). Bioversity International. http://www.euforgen.org/fileadmin//templates/euforgen.org/upload/Publications/Technical_guidelines/Technical_guidelines_Fagus_sylvatica.pdf

Walthert, L., Ganthaler, A., Mayr, S., Saurer, M., Waldner, P., Walser, M., Zweifel, R., & von Arx, G. (2021). From the comfort zone to crown dieback: Sequence of physiological stress thresholds in mature European beech trees across progressive drought. Science of The Total Environment, 753, 141792. https://doi.org/10.1016/j.scitotenv.2020.141792

Wang, Q., Tenhunen, J., Dinh, N. Q., Reichstein, M., Otieno, D., Granier, A., & Pilegarrd, K. (2005). Evaluation of seasonal variation of MODIS derived leaf area index at two European deciduous broadleaf forest sites. Remote Sensing of Environment, 96(3), 475–484. https://doi.org/10.1016/j.rse.2005.04.003

Wang, Y. P., Lu, X. J., Wright, I. J., Dai, Y. J., Rayner, P. J., & Reich, P. B. (2012). Correlations among leaf traits provide a significant constraint on the estimate of global gross primary production. Geophysical Research Letters, 39(19). https://doi.org/10.1029/2012GL053461

Weithmann, G., Link, R. M., Banzragch, B.-E., Würzberg, L., Leuschner, C., & Schuldt, B. (2022). Soil water availability and branch age explain variability in xylem safety of European beech in Central Europe. Oecologia, 198(3), 629–644. https://doi.org/10.1007/s00442-022-05124-9

Wilkening, J. V., Skelton, R. P., Feng, X., Dawson, T. E., & Thompson, S. E. (2023). Exploring within-plant hydraulic trait variation: A test of the vulnerability segmentation hypothesis. Plant, Cell & Environment, 1–21. https://doi.org/10.1111/pce.14649

Willigen, C. V., Sherwin, H. W., & Pammenter, N. W. (2000). Xylem hydraulic characteristics of subtropical trees from contrasting habitats grown under identical environmental conditions. The New Phytologist, 145(1), 51–59. https://doi.org/10.1046/j.1469-8137.2000.00549.x

Wullschleger, S. D., Epstein, H. E., Box, E. O., Euskirchen, E. S., Goswami, S., Iversen, C. M., Kattge, J., Norby, R. J., van Bodegom, P. M., & Xu, X. (2014). Plant functional types in Earth system models: Past experiences and future directions for application of dynamic vegetation models in high-latitude ecosystems. Annals of Botany, 114(1), 1–16. https://doi.org/10.1093/aob/mcu077

Xie, S., Mo, X., Liu, S., & Hu, S. (2023). Plant Hydraulics Improves Predictions of ET and GPP Responses to Drought. Water Resources Research, 59(5), e2022WR033402. https://doi.org/10.1029/2022WR033402

Xu, H., Wang, H., Prentice, I. C., Harrison, S. P., & Wright, I. J. (2021). Coordination of plant hydraulic and photosynthetic traits: Confronting optimality theory with field measurements. New Phytologist, 232(3), 1286–1296. https://doi.org/10.1111/nph.17656

Xu, X., Medvigy, D., Powers, J. S., Becknell, J. M., & Guan, K. (2016). Diversity in plant hydraulic traits explains seasonal and inter-annual variations of vegetation dynamics in seasonally dry tropical forests. New Phytologist, 212(1), 80–95. https://doi.org/10.1111/nph.14009

Yao, Y., Joetzjer, E., Ciais, P., Viovy, N., Cresto Aleina, F., Chave, J., Sack, L., Bartlett, M., Meir, P., Fisher, R., & Luyssaert, S. (2022). Forest fluxes and mortality response to drought: Model description (ORCHIDEE-CAN-NHA r7236) and evaluation at the Caxiuanã drought experiment. Geoscientific Model Development, 15(20), 7809–7833. https://doi.org/10.5194/gmd-15-7809-2022

Zapater, M., Hossann, C., Bréda, N., Bréchet, C., Bonal, D., & Granier, A. (2011). Evidence of hydraulic lift in a young beech and oak mixed forest using 18O soil water labelling. Trees, 25(5), 885. https://doi.org/10.1007/s00468-011-0563-9

Zhang, Y., Narayanappa, D., Ciais, P., Li, W., Goll, D., Vuichard, N., De Kauwe, M. G., Li, L., & Maignan, F. (2022). Evaluating the vegetation–atmosphere coupling strength of

ORCHIDEE land surface model (v7266). Geoscientific Model Development, 15(24), 9111–9125. https://doi.org/10.5194/gmd-15-9111-2022

Table 1. Summary of the environmental characteristics of each experimental site. All data is based on Poyatos et al. (2021) except those explicitly mentioning the source.

	DE-Hin	ES-Alt	FR-Hes	FR-Pue
Country	Germany	Spain	France	France
Site Name	Hinnensee	Alto Tajo	Hesse	Puechabon
Latitude (°)	53.33	40.802	48.674	43.741
Longitude (°)	13.192	-2.230	7.065	3.596
Elevation (m a.s.l.)	90	981	300	270
Mean Annual Precipitation (mm yr^{-1})	606.40	566.90	1003.48	1022.97
Mean Annual Temperature (°C)	8.68	11.74	9.97	13.80
Köppen-Geiger Climate Classification (Beck et al., 2018)	Cfb	Csb	Cfb	Csa
Slope (%)	2-5	5-10	0-2	0-2
Soil Texture	Sandy	n.a.	Silty	Clay-Loam
Soil Depth (cm)	n.a.	n.a.	120	52.5
Species under analysis	*Fagus sylvatica*	*Quercus ilex*	*Fagus sylvatica*	*Quercus ilex*
Stand Age (yr)	~200	59	34	58
Stand Basal Area (m^2 ha^{-1})	n.a.	13.1	19.7	28.1
Stand Height (m)	24.0	4.9	13.0	5.0
Period of Analysis	2012-2014	2012-2014	2001-2005	2001-2005

Table 2. Plant hydraulic parameterization (i.e., k_{max}, Ψ_{p50}, and c_k) used for the three numerical experiments carried out in each experimental site. The k_{max} used in experiment 3 was selected independently for each site after experiment 2. The plant hydraulic parametrization does not differ between plant segments (i.e., roots, stem, leaves) within the same tree species and configuration.

Experiment	Plant Hydraulic configuration	Parameter	Units	*Fagus sylvatica*	*Quercus ilex*
Experiment 1	Default Model Configuration (DC)	k_{max}	mm_{H2O} $mm_{H2O}^{-1}s^{-1}$	2×10^{-8}	
		c_k	-	3.95	
		Ψ_{p50}	MPa	-2.7	
	Vulnerable Tree Configuration (VC)	k_{max}	mm_{H2O} $mm_{H2O}^{-1}s^{-1}$	2×10^{-8}	
		c_k	-	1.73	1.06
		Ψ_{p50}	MPa	-1.9	-4.97
	Resistant Tree Configuration (RC)	k_{max}	mm_{H2O} $mm_{H2O}^{-1}s^{-1}$	2×10^{-8}	
		c_k	-	3.33	2.27
		Ψ_{p50}	MPa	-4.7	-7.66
Experiment 2	All configurations	c_k	-	3.95	
		Ψ_{p50}	MPa	-2.7	
	Hk_{max}	k_{max}	MPa	2.0×10^{-7}	
	IHk_{max}	k_{max}	MPa	1.1×10^{-7}	
	DCk_{max}	k_{max}	MPa	2.0×10^{-8}	
	ILk_{max}	k_{max}	MPa	1.1×10^{-8}	

	Lk_{max}	k_{max}	MPa	2.0 x 10^{-9}	
Experiment 3	Default Model Configuration (DC)	k_{max}	mm_{H2O} $mm_{H2O}^{-1}s^{-1}$	1.1 x 10^{-8}	1.1 x 10^{-8} (FR-Pue) 6.5 x 10^{-8} (ES-Alt)
		c_k	-	3.95	
		Ψ_{p50}	MPa	-2.7	
	Vulnerable Tree Configuration (VC)	k_{max}	mm_{H2O} $mm_{H2O}^{-1}s^{-1}$	1.1 x 10^{-8}	1.1 x 10^{-8} (FR-Pue) 6.5 x 10^{-8} (ES-Alt)
		c_k	-	1.73	1.06
		Ψ_{p50}	MPa	-1.9	-4.97
	Resistant Tree Configuration (RC)	k_{max}	mm_{H2O} $mm_{H2O}^{-1}s^{-1}$	1.1 x 10^{-8}	1.1 x 10^{-8} (FR-Pue) 6.5 x 10^{-8} (ES-Alt)
		c_k	-	3.33	2.27
		Ψ_{p50}	MPa	-4.7	-7.66